Specialized replication mechanisms maintain genome stability at human centromeres

Andrea Scelfo[1*], Annapaola Angrisani[1*], Marco Grillo[1], Bethany M. Barnes[2], Francesc Muyas[3], Carolin M. Sauer[3], Chin Wei Brian Leung[4], Marie Dumont[1], Marine Grison[1], David Mazaud[5,6], Mickaël Garnier[5,6], Laetitia Guintini[7], Louisa Nelson[2], Fumiko Esashi[4], Isidro Cortés-Ciriano[3], Stephen S. Taylor[2], Jérôme Déjardin[7], Therese Wilhelm[1,#] and Daniele Fachinetti[1,#]

[1]Institut Curie, PSL Research University, Sorbonne Université, CNRS, UMR 144, 26 rue d'Ulm, Paris 75005, France.

[2]Division of Cancer Sciences, School of Medical Sciences, Faculty of Biology, Medicine and Health, University of Manchester, Manchester Cancer Research Centre, Wilmslow Road, Manchester M20 4GJ, United Kingdom.

[3]European Molecular Biology Laboratory, European Bioinformatics Institute, Hinxton, Cambridge CB10 1SD, United Kingdom.

[4]Sir William Dunn School of Pathology, University of Oxford, Oxford, OX1 3RE, United Kingdom.

[5]Plateforme Imagerie PICT-IBiSA, Institut Curie, PSL Research University, Paris 75005, France.

[6]Institut Curie, PSL Research University, Sorbonne Université, CNRS UMR3664, Paris 75005, France.

[7]Institute of Human Genetics, CNRS-Université de Montpellier, Montpellier 34396, France.

*These authors contribute equally

#Co-corresponding authors: therese.wilhelm@curie.fr; daniele.fachinetti@curie.fr

Lead Contact: daniele.fachinetti@curie.fr

Keywords: Genome Instability, Replication stress, centromere, DNA replication, proteomics, DNA damage

Summary

The high incidence of whole-arm chromosome aneuploidy and translocations in tumors suggests instability of centromeres, unique loci built on repetitive sequences and essential for chromosome separation. The causes behind this fragility and the mechanisms preserving centromere integrity remain elusive. We show that replication stress, hallmark of pre-cancer lesions, promotes centromeric breakage in mitosis, due to spindle forces and endonuclease activities. Mechanistically, we unveil unique dynamics of the centromeric replisome distinct from the rest of the genome. Locus-specific proteomics identifies specialized DNA replication and repair proteins at centromeres, highlighting them as difficult-to-replicate regions. The translesion synthesis pathway, along with other factors, act to sustain centromere replication and integrity. Prolonged stress causes centromeric alterations like ruptures and translocations, as observed in ovarian cancer models experiencing replication stress. This study provides unprecedented insights into centromere replication and integrity, proposing mechanistic insights into the origins of centromere alterations leading to abnormal cancerous karyotypes.

Introduction

Genomic instability is an early event of cell transformation. It spans from chromosomal alterations to changes in chromosome numbers. Whole-arm chromosome aneuploidy (gain, loss) and translocations are common features of cancer[1-3]: they are present since the initial stages of tumour formation and increase as the disease progresses[4]. This type of alteration is likely triggered by an initial break event occurring within the (peri-) centromeres, regions of each chromosome which cover 3–5% of total human genome[5,6] that are essential for proper chromosome separation during cell division[7]. Their key role in cell division suggests the existence of specialized mechanisms to maintain their integrity, nevertheless centromeres have been found to be intrinsically fragile[8-13]. The molecular basis of this observed fragility and what preserves proper centromeric stability are currently unknown.

Human centromeres are mid-to-late replicating regions[14-16] built over megabase-length, AT-rich repetitive sequences prone to form non–B-DNA structures[7,17,18] and DNA:RNA hybrids[11,19,20]. These features resemble those of common fragile sites (CFSs), difficult-to-replicate regions that undergo stress-dependent chromosome breakage in mitosis[21]. This suggests that centromeres might undergo particularly challenging DNA replication that, when further perturbed, could lead to ruptures and chromosomal rearrangements (**Figure 1A**).

Human centromeres are hot spots for ruptures under replication stress

To directly assess if perturbation of DNA replication promotes centromere breakage, we analyzed the presence of centromere ruptures after low-dose (200 nM) and short (24 h) treatment with Aphidicolin (APH), a DNA polymerases α/δ/ε inhibitor, in non-transformed diploid RPE-1 cells. We scored for breakages in metaphase either in asynchronous cells or in cells arrested in mitosis with the APC/CDC20 inhibitors ProTAME/Apcin (P/A)[22]. The prolonged microtubule pulling on the centromere/kinetochore structure with the P/A treatment was chosen to better reveal and/or promote centromere fragility due to the possible presence of unreplicated DNA or other abnormal structural variations at centromeres (**Figure S1A**). APH treatment doubled the formation of ruptures at centromeres, and this was further exacerbated by prolonged microtubule pulling (P/A) specifically at centromeric regions (**Figure 1B, C** and **S1B, C**). Accordingly, phosho-Ser139 on histone H2A.X (γH2A.X) and 53BP1 foci accumulation, used as markers for damage/stress, increased by more than 2-fold at mitotic or interphase centromeres, respectively, in APH-treated cells compared to not treated (NT) (**Figure S1D, E**). A similar increase in centromere breaks compared to non-centromeric regions was observed by reducing the nucleotide pool in Hydroxyurea (HU)-treated cells (**Figure S1F**). Multicolour FISH (mFISH) analysis further revealed that some centromeres are more fragile than others, in particular centromeres of chromosomes 1, 2, 5, 11 and X were significantly susceptible to break under replication stress (RS) conditions (**Figure 1D, E** and **S1G**).

We then investigated for an active mechanism that induces centromere cleavage besides the observed mechanical stress due to prolonged microtubule pulling on the centromere/kinetochore structure. We tested the presence of MUS81, a structure-specific endonuclease known to cleave under-replicated DNA that persists at CFS until mitosis[23,24]. The recruitment of the MUS81 endonuclease to centromeres increased by more than 4-fold in APH-treated cells and coincided with γH2A.X at centromeres in mitotic cells (**Figure 1F**). Reduction of MUS81 levels by RNAi (**Figure S1H**) significantly decreased the formation of centromere breaks in APH-treated cells (**Figure 1G** and **S1I**). This indicates that cleavage of centromeres by the structure specific endonuclease MUS81 accounts at least partially for the observed centromere breaks and suggests that centromeres are sites of unfinished replication in mitosis.

Finally, we determined the timing of DNA damage accumulation at centromeres under RS. Upon cell cycle synchronization in G1 and release (**Figure S1J**), we observed γH2A.X foci accumulating at centromeres in mid/late S-phase, which is the time of centromere replication[14-16], in APH-treated cells compared to control (**Figure 1H, I** and **S1K**). Accordingly, single strand DNA (ssDNA) foci, detected by BrdU under non-denaturing conditions, accumulated at higher incidence within centromeric regions during S-phase in basal conditions and upon HU-mediated RS (**Figure 1J**). γH2A.X accumulation decreased in G2 and in the following G1 suggesting partial repair of the lesions. Accordingly, 53BP1 started to accumulate in G2 and became more pronounced in the next G1 after RS (**Figure 1H, I** and **S1K, L**). In conclusion, our data identify a direct correlation between RS, occurrence of DNA damage and breaks at centromeres.

Human centromeres harbor a specialized replication dynamics influenced by secondary structures and ATR activity

To understand the causes of RS-related centromere fragility, we analyzed different DNA replication parameters at centromeres throughout S-phase in RPE-1 cells following G1-release using a single molecule DNA combing approach (**Figure S1J**, and **S2A**). Bulk genome replication proceeded with an average median speed of 1.25 kb/min in early S-phase and increased up to 36% in late S phase (**Figure 2A, B**), in agreement with previous studies[25,26]. In contrast, centromeres replicated at a slower pace at every stage of S-phase (median of 0.97 kb/min in early S) with only a minor increase of 16% towards the end of S (**Figure 2A, B**). Beside replication speed, centromeres differed from the bulk genome also in the distance of origin firing, with centromeres showing almost 2-fold reduction in inter-origin distance (IOD), indicating a higher frequency of origin firing compared to the bulk genome (**Figure 2A, C**).

Following APH treatment, replication velocity decreased both in the bulk genome and centromeres (**Figure 2D**), indicating that centromere replication is at least partially assured by canonical polymerases α, δ and ε [27,28]. However, while IOD significantly decreased by 37% in the bulk genome to compensate for the slow fork speed, at centromeres IOD did not decrease (**Figure 2E**), indicating that origin firing approaches its minimal possible distance and/or that centromeres already utilise most of their potential origins. The latter hypothesis suggests that the high frequency of active origins is an important feature of centromere replication in physiological conditions. To directly test this, we treated cells with low doses of a Cdc7 inhibitor (Cdc7i; XL413) to decrease origin firing[29]. Cdc7-mediated inhibition of origin firing led to high frequency of centromere breakage, that was further enhanced when combined with APH treatment (3-fold increase in APH versus a 6-fold increase with APH+Cdc7i compared with untreated), while ruptures on chromosome arms only modestly increased (**Figure 2F-H** and **S2B, C**). These data indicate that centromeres are particularly susceptible to reduced origin firing and frequent origin activation is required to ensure complete centromere replication.

Being difficult-to-replicate regions and due to their late replication timing, centromeres are known to undergo mitotic DNA synthesis (MiDAS) under certain stress conditions[11] or in chromosomal unstable U-2 OS cells[30] to ensure complete replication. Upon inhibition of MiDAS in G2/M with high doses of APH[31], we observed high levels of centromeric γH2A.X foci in the following G1 (**Figure 2I, J** and **S2D**). These results demonstrate that MiDAS plays an important role in finalizing centromeric DNA replication both in unperturbed and under mild RS conditions.

AT-rich regions are prone to form secondary structures known to be obstacles for DNA polymerases causing frequent fork stalling, like at CFSs[32,33]. Centromeres also harbor secondary structures[17,34] like hairpin structures[35-37] and CENP-B-mediated DNA loops[36]. Using fork asymmetry as indicator for fork stalling, we found that centromeres have a higher propensity to undergo fork stalling than the bulk genome (**Figure S2E**). The presence of secondary structures could cause delay in replication fork progression[18,32]. Accordingly, constitutive CENP-B depletion accelerates replication fork progression at centromeres, without any significant alteration in origin firing (**Figure 3A, B**). This suggests that the high incidence of centromeric origin firing is not a result of slower fork progression, but rather an intrinsic property of centromeric regions. Additionally, we detected a ~2-fold increase in centromere breakage (**Figure 3C**). These findings suggest that, in addition to a role for CENP-B in absorbing microtubule pulling forces during mitosis[36], CENP-B-mediated DNA loops could be an important mechanism to retain a slower replication fork progression at centromeres in order to maintain their integrity. Accordingly, increasing replication fork speed via PARP inhibition (PARPi; Olaparib)[38,39] or Interferon-β (IFNβ) treatment[40], both known to accelerate replication[40,41], led to a specific increase in centromere ruptures (**Figure 3D** and **S3A**) and accumulation of 53BP1 foci in the next interphase (**Figure S3B**). These findings suggest that slow replication fork progression is an important feature of centromeres to ensure their integrity. This could be partially dictated by secondary structures like CENP-B-mediated DNA loops.

We then assessed if the high incidence of breakages at centromeric regions is mainly caused by their repetitive nature. To this end we measured γH2A.X enrichment in RPE-1 cells at a non-repetitive neocentromere on chromosome 4[42] in G1 phase following RS in the previous cell cycle. The artificially generated neocentromere has a CENP-A domain size comparable to that of canonical centromeres and is marked by centromeric proteins (here visualized with ACA antibody) except CENP-B[42], known to bind directly to repetitive DNA sequence[43]. Upon APH-induced RS and Apcin-mediated microtubules pulling (**Figure 3E**), γH2A.X foci accumulated in the next G1 preferentially at canonical repetitive centromeres, indicating that the repetitive DNA sequence enhanced fragility of these sites possibly via replication interference. Interestingly, γH2A.X could still be detected at the repetitive-less neocentromere, possibly due to the mechanical stress experienced during mitosis (**Figure 3F**).

We then assessed what favors the high incidence of origins firing at centromeres. The Ataxia Telangiectasia and Rad3-related protein (ATR) is a well know negative regulator of origins firing[44]. As suggested by *in vitro* reconstituted centromeric DNA replication, ATR activity could be limited at centromeres[45]. To address if the attenuation of ATR activity might be a mechanism contributing to the elevated frequency of centromeric origin firings, we artificially tethered the ATR activator ETAA1[46] to centromere by fusing it with the DNA binding domain of CENP-B (referred to CB-DBD) (**Figure 3G** and **S3C**), as we have previously done to reduce centromeric instability by mitigating centromeric R-loops formation[11]. We used super resolution microscopy (STORM) to determine replication dynamics at single molecule level[47]. To better control its expression and activity we used a doxycycline-inducible ETAA1$^{\text{CB-DBD}}$ coupled with the auxin-inducible degron (AID)[48] to mediate its degradation (**Figure S3D**). As expected by having active ATR[49], expression of ETAA1$^{\text{CB-DBD}}$ led to accumulation of γH2A.X specifically at centromeres (**Figure 3H**). By calculating the area of EdU signal at the centromere over the whole centromeric area (marked by ACA), we revealed a significant decrease in EdU incorporation specifically at centromeres following dox-induction of ETAA1$^{\text{CB-DBD}}$ (**Figure 3I** and **S3E**). This reduction was similar to the one scored upon inhibition of Cdc7, which, contrarily to ETAA1$^{\text{CB-DBD}}$, impacted also non-centromeric regions (**Figure 3I** and **S3E**). Inhibition of ATR (VE-821) restored the EdU signal of dox-treated cells to normal level (**Figure 3I**), confirming the specificity of the system. This alteration in replication dynamics correlated with accumulation of 53BP1 foci and presence of DNA breaks following induction of ETAA1$^{\text{CB-DBD}}$ (**Figure 3J, K**). Altogether, since ATR is known to regulate origin firing and the decrease in EdU area/signal was comparable to the condition of Cdc7 inhibition, our data suggest that the high incidence of origin firing at centromeres (**Figure 2C**) is likely due to the local restrained activity of ATR. This is necessary to guarantee completion of centromere replication and to prevent centromere breakages.

Specialized protein network at human centromeres

The high frequency of active replication origins at centromeres indicates high incidence of replication fork convergence with accumulation of topological stress[50]. To understand the repertoire of proteins granting proper centromere replication and coping with replication termination dense regions, we performed a quantitative locus-specific proteomic analysis (Proteomics of Isolated Chromatin, PICh[51,52], see Star Methods). The use of a combination of six human centromere-specific probes[11] allowed us to isolate and purify centromeric chromatin from human cells, whose composition was then analyzed by Mass Spectrometry (**Figure 4A, B**). A total of 2145 proteins were identified and known centromeric factors were among the most abundant ones, therefore validating the specificity of our method (**Figure 4B, C**).

To reveal a specific set of proteins important to maintain centromere integrity, we performed a quantitative PICh through Tandem-Mass-Tag (TMT) Mass Spectrometry in cells suffering from RS and enhanced fragility at centromeres[11,36] hypothesizing that key proteins required for centromere stability would be reduced in these conditions. To this end, we compared RPE-1 cells depleted or not for CENP-B and in which CENP-A can be degraded in an inducible manner by auxin (IAA) addition (^{AID}CENP-A)[53]. Differential proteomics analysis revealed 594 regulated proteins (hits and candidates), with the major changes observed in the CENP-B$^{-/-}$ and CENP-A/-B double depletion cells (**Figure 4D, S4A** and **Table S1**). CENP-A, and to a certain extent CENP-B, are known to play a key role in mediating assembly and maintenance of centromeric and kinetochore components[7,54,55]. Accordingly, we observed a strong reduction of most of these components in CENP-A depleted cells, further enhanced by concomitant CENP-B depletion (**Figure 4E** and **S4B**), validating our comparative analysis.

Functional annotation revealed that ~17% of the hit proteins that change between the analyzed conditions are involved in DNA replication, DNA damage response and DNA repair pathways (**Figure 4F**). Notably, we scored TOP2A/B topoisomerases among the most abundant factors at centromeres (**Figure 4G**), in accordance with their role in resolving topological stress at converging forks[56-58]. Among the hit proteins involved in DNA repair, we found (**Figure 4G**): i) factors necessary for resolution of Ultra Fine Bridges (UFBs) such as BLM, RIF1, FANCD2[59] and TOPBP1, known to act as TOP2A recruiter at UFBs[60] and be important for repair during mitosis[61], confirming the presence of topological stress and/or unresolved replication /recombination intermediates at centromere; ii) SLX4 and its interacting partner SLX4IP, recruited by TOPB1[61] and known to enroll MUS81 to sites of under-replicated DNA in mitosis[62,63], thus suggesting the presence of under-replicated DNA at centromeres after RS; iii) factors of the post-replicative repair pathways such as the nucleotide and base excision repairs and the mismatch repair. The mismatch repair complex was previously reported to be associated with centromeric DNA in *Xenopus laevis* egg extract[45] and in meiosis[64], and MSH3 in complex with SLX4 to resolve late recombination intermediates[65]; iv) SLF1 and SLF2 serving as SMC5/6 recruiters at genomic loci presenting DNA lesions that can interfere with progression of the DNA replication machinery[66]. SLF1/SLF2 form a complex with RAD18[66], a E3 ubiquitin-protein ligase acting on PCNA Lys164 monoubiquitination (PCNA-Ub1)[67]. This PCNA modification is the molecular trigger to switch from the replicative polymerase to a set of specialized but low-fidelity error-prone polymerases, in order to allow the replisome to progress while tolerating DNA damage[68]. Accordingly, we found most of the polymerases and accessory factors involved in the translesion synthesis pathway (TLS) (**Figure 4G**). Overall, the observed presence at centromeres of a substantial pool of proteins involved in DNA damage and repair, suggests that these factors cooperatively act at centromeric regions to assist replication and maintain genome stability.

TOP2A and SMC6 preserve centromere stability

Topoisomerase TOP2A and SMC5/6 were already reported to reside at centromeres[69-71] and to act at replication termination sites[56-58,72]; however, their role in the maintenance of centromere integrity remains still unexplored. To test their function during centromeric DNA replication, we depleted TOP2A or SMC6 in mid-S phase in pseudo-diploid HCT116 cancer cells (**Figure 5A** and **S5A, B**) using already established Auxin-inducible degron cell systems[69,73]. We assessed centromere breaks in P/A metaphase-arrested cells and post-replicative 53BP1 foci accumulation at centromeres in the following G1 (**Figure 5A**). Besides inducing highly decondensed chromosomes[71] and P/A treatment being less effective in HCT116 cells than RPE-1 cells, TOP2A depletion in HCT116 cells caused a 2-fold increase in gaps/breaks at both centromeric and non-centromeric regions and increased centromeric 53BP1 foci in the following G1 (**Figure 5B, C** and **S5C, D**). Single depletion of SMC6 or co-depletion of its partner NSE4A during S-phase also led to a similar increase in centromere and non-centromeric breakage (**Figure 5C, D** and **S5D-F**). The breaks observed outside the centromeric regions in SMC6-depleted HCT116 often coincided with the CFS FRA3B and FRA4D, highlighting similarities between centromeres and CFSs (**Figure S5G**).

To define whether TOP2A and SMC6 act in centromere replication or in a post-replicative manner, we challenged untreated or IAA-treated cells with Calyculin A, a PP1/PP2A phosphatase inhibitor that promotes premature and rapid condensation of interphase-chromatin[74] (**Figure S5H, I**). This reveals DNA breaks at active replicating regions in mitotic-like chromosomes. In this condition, an increase of centromeric ruptures in the absence of TOP2 or SMC6 was scored (**Figure S5J**), suggesting that TOP2A and SMC6 can act during DNA replication, likely during termination.

The translesion synthesis pathway contributes to centromere replication

Translesion polymerases are able to maintain ongoing DNA replication even in the presence of lesions, thus guaranteeing overall genome replication[75]. Polζ has been previously reported to play an important role for DNA replication and repair at pericentromeric regions in murine cells[76]. Using a doxycycline inducible shRNA system to downregulate REV3L (the catalytic subunit of Polζ) (**Figure S5K**), we found that replication of human centromeres is also impaired, causing replication progression delay at centromeres compared with the bulk genome, with a slight increase in origin firing (measured as number of ongoing forks/100 kb) **(Figure 5E, F** and **S5L)**. These mild alterations in replication fork dynamics were nevertheless sufficient to promote an increase in ruptures and 53BP1 foci accumulation specifically at centromeres (**Figure 5G, H** and **S5M**). These results were further confirmed using an inhibitor of REV1/REV7 interaction (JH-RE-06), impairing Polζ recruitment[77] (**Figure 5G, H** and **S5M**).

Our findings suggest that canonical polymerases assure major centromere replication but the translesion polymerase complex could intervene in presence of lesions. Accordingly, centromeric breakages slightly increased by co-inhibition of DNA polymerases α/δ/ε (*via* 100 nM APH) and Polζ (*via* shRNA or JH-RE-06), while non-centromeric regions remained mainly unperturbed (**Figure S5L**). The cooperation between canonical DNA polymerases and the translesion polymerase Polζ in safeguarding replication at centromere was also observed during MiDAS (**Figure 5I**). Taken together, our findings indicate that TLS plays a role for centromere replication and overall centromere integrity.

Centromere alterations are prominent in tumors and are caused by long-term replication stress

We then determined whether centromere fragility is a feature of the tumor cell landscape. To this end we analyzed the copy number alterations (CNAs) that fell within the centromeric regions (± 50 Kb) in a cohort of 2897 tumour samples, derived from 33 different cancer types, available on The Cancer Genome Atlas (TCGA) database[78] (**Figure 6A, B** and **Table S2**). CNAs falling within centromeric loci were observed throughout all types of cancers, with a higher frequency in some tumour types (**Figure 6B**). We integrated this computational pan-cancer data with the analysis of a panel of 31 *ex-vivo* ovarian cancer models (OCMs) – tumour cell cultures from 21 patients with ovarian cancer isolated from solid biopsies and ascites[79-81]. 17 patients were diagnosed with high-grade serous ovarian cancer (HGSOC), a disease characterised by *TP53* mutation and extensive structural genomic variation (SGV), with the latter often derived from oncogene-induced RS[79]. This cohort also includes two mucinous and four low-grade serous OCMs (LGSOC; from two patients[82]), distinct diseases characterized by low-level of SGV and K-Ras activation[83] and/or activating mutations in protein kinase pathway genes[84], both known to induce RS[85]. Using pseudo-bulked shallow single-cell whole-genome sequencing (scWGS)[80,81], we applied a bioinformatic approach to score for breakpoints (determined by variation in the read-depth[86] that fell within centromeric regions, ± 5 Mb as described in [5]). Breaks within these regions were found in all analyzed OCMs and accounted for up to 63.6% of total breaks with higher frequency in the LGSOC OCMs (**Figure 6C**). Breakpoints were significantly enriched at the centromeres of several chromosomes (3, 5, 6, 8, 16, 19, 20) when compared with the expected number of breaks within a genomic region with the same size of the centromere (**Figure 6D, E**).

To reveal the presence of whole-arm chromosome translocations (WACT) not detectable by scWGS, we performed mFISH in combination with centromeric FISH to identify this type of event in two OCMs of LGSOC and one HGSOC that showed the presence of peri/centromeric breakpoints (**Figure 6C** and **S6A**). In all three cases, besides whole arm chromosome aneuploidies several and recurrent WACTs were detected in the tumoral but not in the corresponding stroma sample (visualized by mFISH or by unmatched scWGS[81]) (**Figure 6G, G** and **SB, C**), highlighting a link between centromere rupture and WACT.

Finally, we directly tested if centromere alterations, WACTs and genomic instability can be promoted by short or long-term perturbation of DNA replication and raised by several cycles of unfinished replication, breakage and incorrect repair, as observed in cancer[87]. We used either RPE-1 cells treated with low dose of APH (200 nM) and Cdc7 inhibitor (10 μM) for 2 days or shRNA-p53 RPE-1 cells treated with very low dose of APH (100 nM) for 8 and 16 days and performed mFISH/α-sat FISH in P/A-arrested cells. We only observed mild variations in the abundance of chromosome-specific centromeric DNA and presence of WACT or aneuploidy after 48 h of treatment (**Figure 6H-J** and **S7A, B**). This is in agreement with the cen-co-FISH analysis, used to reveal centromere instability and recombination[88], showing alterations in the centromeric signals occurring only after 48 h of APH or APH/CDC7i-treated cells (**Figure S7C**). On the contrary, prolonged RS (8 and 16 days) enhanced variation in the abundance of chromosome-specific centromeric DNA, presence of centromeric translocations, and generated high level of aneuploidy (**Figure 6H-J** and **S7A, B)**. Our results establish a direct link between RS and centromere alterations through enhanced recombination. This further exacerbates centromere-related chromosome translocations via incorrect repair and overall genome instability.

Discussion

Mis-regulation of DNA replication is a main driver of genome instability and chromosome ruptures, overall promoting precancerous lesions[89]. RS-dependent chromosome breakage was shown to occur at certain genomic regions, such as CFSs, characterized by one (or more) specific feature(s): late replication, reduced DNA replication initiation events, formation of DNA secondary structures, high levels of transcription and R-loop formation[90]. Human centromeres bear several of these features at once, but despite this, they are quite resistant to breaks and recombination in physiological conditions. Our work demonstrates that centromeres are indeed difficult-to replicate regions, that albeit harbor specialized DNA replication dynamics and mechanisms necessary to maintain their integrity (**Figure 7**). However, they are extremely sensitive to slight perturbations of regulation of their replication. This could explain, at least in part, the high frequency of centromeric alterations observed in cancer cells characterized by high RS[9].

Our data reveal that centromeres replicate at slower speed and increased origin firing compared to the bulk genome (**Figure 7**), requiring mitotic DNA synthesis and TLS polymerase switch to complete their replication. We speculate that this different regulation is a feature of centromeres acquired during evolution due to their repetitive nature and intrinsic structure. While the repetitive nature is an essential feature of centromeres needed for their proper functioning during mitosis[36,91], it could also be the major driver of centromeric instability. Indeed, we demonstrate that repetitive centromeres are more prone to breakage compared to a non-repetitive human centromere, likely via interference of replication fork progression. The slower speed of the advancing replisome can be due to secondary structures present at centromeres, such as the CENP-B-mediated DNA loops[36], accumulation of RNA loops, increased topological stress and overall complex DNA topology[90,92]. However, the high incidence of origin firing at centromeres cannot be explained by a simple correlation between origin firing and fork speed[93] (as observed at some CFS such as FRA16C [94,95]), as suggested by our data on centromere replication dynamics in *CENP-B* KO cells. Rather, we show that the elevated frequency of origin firing is due to a restrained activity of ATR at centromeres since alterations of centromere-specific ATR activity lead to DNA damage. This makes the centromere a dense region of converging forks, overall generating a heavy topological burden. Given all these characteristics, even slight alterations of replication dynamics have profound detrimental effects on centromere integrity, more than on other regions of the genome (**Figure 7**). Whereas slow replication speed could lead to unreplicated DNA, fast progressing forks might increase the topological burden in a termination-dense region. Here we propose that, due to their known activity[58,69,96-98], TOP2A and SMC5/6 complex act at the centromere to resolve topological stress generated by converging forks and/or to facilitate fork restart from stalling during termination (**Figure 7**).

DNA entanglements, under-replicated structures, and recombination intermediates exist at centromere and may generate a low basal DNA damage[90]. Proteins involved in DNA repair, resolution of UFBs, specialized endonucleases and replication proteins were indeed previously found at centromeres[76,94,99]. These observations are corroborated by our data demonstrating the accumulation of ssDNA preferentially at centromeres and the MUS81-dependent cleavage of unreplicated structures. Given that ATR plays a role in suppressing ssDNA formation during DNA replication, the absence of ATR at centromere could generate more ssDNA at stressed forks and this might result in replication forks cleavage[100]. Further, we show that the low-fidelity translesion polymerases are active players in centromeric DNA replication, which extends to MiDAS. This ensures the completion of the challenging centromere replication, even in presence of a low basal DNA damage.

Relying on error-prone TLS polymerases in order to limit the risk of fork collapse can contribute to an increased frequency of mutagenic events, especially at late-replicated regions that *per se* present higher rates of spontaneous mutagenesis[101]. However, this can be a minor problem for repetitive, non-coding sequences like centromeres and could contribute to the extensive variability of these regions[102]. The proneness of centromeres to mutations and cycles of breakage, repair and recombination may be the cause of their evolutionary dynamism and diversity between individuals[5].

The challenges that centromeres face during replication, together with the high level of mechanical stress that the centromere/kinetochore needs to support during chromosome segregation, suggest that centromeres are even more fragile than CFSs when under stress. While CFSs cleavage is required to preserve the genome integrity[24], ruptures and incorrect repair at centromere will inevitably lead to whole-arm chromosome rearrangements and aneuploidy[90]. Indeed, our results directly demonstrate that RS-mediated DNA damage causes instability of centromeric repeats promoting WACTs, likely due to incorrect repair and recombination among repeats, further causing reduced centromere function and consequently aneuploidy. Centromere breakages may initially halt cell proliferation by activating the cell cycle checkpoints, but rearrangements involving centromeres might become tolerated and prominent in cancerous lesions[3,103], as we observed in ovarian cancers characterized by recurrent WACTs. Here, we propose that centromeres are among the most susceptible regions to RS; therefore, early signatures of WACTs could highlight the presence of RS that sets the basis of pre-cancerous lesions and could potentially serve as a biomarker for assessing tumour grade. Moreover, we speculate that centromere fragility could be leveraged in chromosome instability-inducing therapies to potentially limit cellular transformation and cancer progression.

In summary, our work provides and establishes a novel link between centromere DNA replication and fragility and aneuploidy, with the intent to open novel avenues for the development of therapeutic approaches in cancer treatment.

Limitations of the study

The study of replication dynamics at centromeres is limited to one diploid human cell line (RPE-1). We cannot exclude that other non-transformed cell types and cancer cell lines have a different replication behavior. Similarly, the proteomics of centromeres was only carried out in RPE-1 and the role of SMC5/6, TOP2A and TLS complex was only tested in two human cultured cell backgrounds (RPE-1 and/or HTC-116, a near diploid colon cancer line).

Acknowledgements. We thank all the members of the Fachinetti, Tran, Basto, Ceccaldi, Bardin and Chen teams at Institut Curie for discussion. We thank Mandy Rattel and Frank Stein at the Proteomics Core Facility (EMBL, Heidelberg) for the Mass Spectrometry data. We acknowledge Lorenza Penengo (U. of Zurich, Switzerland), Philippe Pasero (IGH, France) and Cristina Bartocci

(I. Curie) for suggestions; Masato Kanemaki (National Institute of Genetics, Japan), Lars Jansen (U. of Oxford, UK), Benoit Le Tallec (ENS, France) and Vincenzo Costanzo (IFOM, Italy) for sharing reagents. We acknowledge the Flow Cytometry Core Facility and the Cell and Tissue Imaging facility (PICT-IBiSA, member of the French National Research Infrastructure France-BioImaging ANR10-INBS-04) of the Institut Curie.

Funding: D.F. receives salary support from the CNRS. D.F. has received support for this project by Labex « CellnScale», the Institut Curie, the program «Investissements d'Avenir» launched by the French Government and implemented by ANR with the references ANR-10-LABX-0038 and ANR-10-IDEX-0001-02 PSL, the Émergence(s) grant 2018 from the city of Paris, ANR-17-CE12-0003, INCa PLBIO21-012 16067. A.S. was supported by AIRC and from the European Union's Horizon 2020 research and innovation program under the Marie Skłodowska-Curie grant agreement No. 800924. A.A. was supported by Italian Pasteur Institut-Cenci Bolognetti Foundation, Rome. B.M.B, L.N, S.S.T are funded by Cancer Research UK Programme Grant (A31334) awarded to S Taylor. F.M., C.S. and I.C.-C. thank EMBL for funding.

Author contributions: T.W, A.S., A.A., M.G., M.G., M.D., L.N., C.W.B.L. and D.F. obtained the experimental data and interpreted the results; B.M.B., F.M. and C.M.S. performed sequencing analysis; L.G. provided key technical expertise supervised by J.D.; D. M. and M. G. performed STORM analysis; T.W, A.S., A.A. and D.F. designed the experiments. T.W. and D.F. conceptualized the project. D.F., J.D., F.E., S.S.T. and I.C-C. obtained funding. D.F. supervised the experimental work. T.W., A.S. and A.A D.F. drafted the manuscript All authors participated in reviewing and editing the manuscript.

Declaration of Interests

The authors declare no competing interests.

FIGURE LEGENDS

Figure 1. Human centromeres are hotspots for ruptures under replication stress.

A. Schematic of the scope of the manuscript.

B. Representative images of centromeric FISH on chromosome spreads from ProTAME/Apcin treated RPE-1 cells. Arrows indicate centromeric breaks after 24h APH-induced RS (200nM). Asterisk marks a non-centromere break. Scale bar = 5 µm.

C. Centromeric breaks quantification per observed metaphase in the indicated conditions. The fractions of analyzed metaphases showing 0, 1 and ≥2 centromere breaks are represented. N = 3, n = 26-92 analyzed metaphases (table S3). Error bars represent the standard error of the mean (SEM). χ^2 test (breaks vs non-breaks) **p = 0.0021, 0.0033; ****p < 0.0001.

D. Representative images of mFISH followed by a centromeric FISH of non-treated (NT) and APH-treated (24h) RPE-1 cells with P/A treatment (3h). Arrows indicate centromeric breaks. Scale bar = 5 µm.

E. Percentage of centromeric breaks observed at specific chromosomes in NT and APH-treated RPE-1 with P/A treatment (3h). Bars show the mean of three experiments, n = 36-52 (table S3); error bars represent SEM. χ^2 test (breaks vs non-breaks) p: 0.05 < *, **: 0.001 < p < 0.01.

F. Representative immunofluorescence image of MUS81, γH2A.X and CENP-C staining on metaphase spread (left panel), and quantification of colocalizing foci per metaphase in untreated (NT) and APH-treated cells (200 nM, 24h), (right panel). Each dot represents one experiment depicted with a different shape (N = 3, n = 29-45 analyzed metaphases/experiment, see table S3); error bars represent SEM. Unpaired t-test *p = 0.0379. Scale bar = 2 μm.

G. Centromeric breaks quantification per observed metaphase in MUS81-depleted cells compared to a scrambled control. The fractions of analyzed metaphases showing 0, 1 and ≥2 centromere breaks are represented. N = 3, n = 65-71 analyzed metaphases/experiment (table S3); error bars represent SEM. χ^2 test (breaks vs non-breaks) ***p = 0.0002.

H. Schematic of the experiment shown in I. W/O: washout

I. Quantification of centromeric γH2A.X and 53BP1 foci at different cell cycle phases in synchronized RPE-1 cells untreated and APH-treated (200 nM) following G1 release (Palbociclib washout); to block cells in the next G1, Palbociclib was added during G2. As NT and APH treatment showed different cell cycle progression, we compared 8 h NT vs 12 h APH (S phase), 12 h NT vs 24 h APH (G2 phase). Dots represent the mean of 3 or 6 experiments and error bars represent the SEM (table S3). n = an average of > 40 cells/experiment was analyzed for condition. Unpaired t-test ***p = 0.0032, 0.0211

J. Native BrdU intensity quantification at random or centromeric regions in NT and HU-treated RPE-1 cells. Dots depicted with different shape represent the mean value of one experiment. N = 3, n = 38-157 analyzed S-phase/experiment (table S3); error bars represent SEM. Unpaired t-test *p = 0.0444, 0.0336; **p = 0.0048; ***p < 0.0001.

Figure 2. Specialized replication fork dynamics ensure centromere stability

A. Representative image of a centromeric DNA fiber incorporated with IdU (green) and CldU (red) and hybridized with centromeric DNA probes. Yellow square marks a zoomed region; dotted line indicates the stitching of two adjacent images. Scale bar = 10 μm.

B. Replication fork velocity quantification measured at centromere and bulk DNA at the indicated time after release from G1 arrest by Palbociclib. Dark bars indicate the median, green and blue ranges the median range for centromeres and bulk DNA, respectively. N = 3, n = 73-218 analyzed DNA fibers per condition (table S3). Mann–Whitney U test: ****$p < 0.0001$.

C. Inter-Origin Distance (IOD) expressed in kilobases at centromeres and the bulk genome in Palbociclib-released cells after 6 (early-S phase), 8 (mid-S phase) and 10 h (late S-phase). N = 3, n = 114-253 analyzed DNA fibers. The black bars represent the median. Mann–Whitney U test: ****$p < 0.0001$.

D, E. Quantification of the replication fork velocity (D) and Inter-Origin Distance (E) measured at centromere and bulk DNA in asynchronous cells treated or not (not treated; NT) with APH (200 nM, 24 h). N = 3, n = 50-326 and n = 51-171 analyzed DNA fibers, respectively (table S3). Mann–Whitney U test: ****$p < 0.0001$.

F. Representative images of centromeric FISH of P/A (3h) and APH treated (200 nM, 24h) ± CDC7i in RPE-1 cells (with 3h P/A treatment). Arrows indicate breaks occurring at centromeres. Scale bar = 10 µm.

G. Violin plot showing number of breaks/metaphase at centromeres and chromosome arms in the indicated conditions (with P/A treatment). Dotted lines separate independent experiments. N = 3 and 4, n = 30-86 analyzed metaphases/experiment (see table S3). Unpaired t-test **$p = 0.0020$, ****$p < 0.0001$.

H. Centromeric breaks quantification per observed metaphase in the indicated conditions (with P/A treatment). The fractions of analyzed metaphases showing 0, 1 and ≥ 2 centromere breaks are represented. N = 3 and 4, n = 30-86 analyzed metaphases/experiment (table S3). Dotted lines separate independent experiments. Error bars represent the SEM. χ^2 test (breaks vs non-breaks) ***p = 0.0003, ****p < 0.0001.

I. Schematic of the experiment shown in J.

J. Representative image of centromeric γH2A.X and 53BP1 foci in cells treated as in I upon MiDAS inhibition (left); Scale bar = 5 μm; white squares correspond to the shown insets. Quantification of γH2A.X intensity is shown in the violin plot (right). Dots depicted with different shapes represent the mean value of one experiment. Dark bars indicate the median, dashed lines the interquartiles. N =3, n = 62-118 cells/experiment (table S3). Unpaired t-test **p = 0.0130, ****p < 0.0001.

Figure 3. CENP-B-mediated secondary structures and ATR tune centromeric replication

A. Schematic of the scope of the experiment shown in B.

B. Quantification of the replication fork velocity (left) and IOD (right) at centromere in asynchronous CENP-B WT and CENP-B KO cells. N = 3; for fork speed, n = 248-207 analyzed DNA fibers per respective conditions; for IOD, n=81-75 analyzed DNA fibers per respective conditions (table S3). The black bars represent the median. Mann–Whitney U test: ****p < 0.0001.

C. Centromeric breaks quantification per observed metaphase in WT and CENP-B KO RPE-1 treated or not with P/A (3 h). N = 3, n = 50-100 analyzed metaphases/experiment (table S3); error bars represent the SEM. Unpaired t-test *p = 0.0156, **p = 0.0013.

D. Violin plot showing quantification of breaks at centromeres and chromosome arms per metaphase in untreated and IFNβ (2h treatment and collect after 48h of release) or Olaparib-treated cells (PARPi for 24 h). N = 2 and 3, n = 35-59 analyzed metaphases/experiment (table S3). Unpaired t-test **p = 0.05, ****p < 0.0001.

E. Schematics of the cell synchronization strategy of the experiment shown in F. W/O: washout.

F. Representative image of γH2A.X signal at a neocentromere (ACA positive and CENP-B negative) and centromeres (ACA and CENP-B positive) in cells treated as in E (left); scale bar = 5 μm; yellow squares correspond to the shown insets. Quantification of γH2A.X per cell is quantified in the bar plot (left). N = 3, n = > 48 analyzed nuclei/experiment (table S3); error bars represent the SEM. Unpaired t-test *p = 0.0151

G. Schematic of the scope of the experiment shown in H, I.

H. Violin plot showing quantification of γH2A.X signal intensity at centromeres and random regions in RPE-1 cells expressing ETAA1$^{\text{CB-DBD}}$ protein tethered to centromere (dox for 48h) compared to IAA-treated control. Dots depicted with different shapes represent the mean value of one experiment. Dark bars indicate the median, dashed lines the interquartiles. N = 3, n = 29-106 analyzed nuclei/experiment (see table S3). Unpaired t-test ****p < 0.0001.

I. Representative STORM microscopy image of EdU signal at centromere (left). White dotted circles mark centromeres that are in focus and analyzed for EdU signal. In the zoomed image, the red area represents EdU covering a centromere. EdU area quantification at centromere is shown on the right. Cells were treated for 24 h. Dots depicted with different shapes represent the mean value of one experiment. N = 3, n = > 5 analyzed cells; error bars represent the error to the mean for one condition (see Methods). Holm post hoc test: ** = 0.001; *** < 0.001.

J. Violin plot showing quantification of centromeric 53BP1 foci per nucleus in RPE-1 cells expressing ETAA1$^{\text{CB-DBD}}$ protein tethered to centromere (dox for 48h) compared to IAA-treated control. Dots depicted with different shapes represent the mean value of one experiment. N = 3, n = > 40 analyzed cells/experiment (table S3). Unpaired t-test ****p < 0.0001.

K. (Left) Representative images of centromeric FISH on chromosome spreads from RPE-1 cells treated with dox for 48h and then ProTAME/Apcin (P/A). Arrows indicate centromeric breaks. Scale bar = 5 µm. (Right) Violin plot showing quantification of centromeric breaks. N = 3, n = ~ 30 analyzed metaphases. Unpaired t-test ****p < 0.0001.

Figure 4. Specialized protein network at human centromeres

A. Schematic illustration of the Proteomics of Isolated Chromatin (PICh) procedure.

B. Silver Staining of centromeric PICh and relative immunoblot analyses with the indicated antibodies.

C. Scatter plot showing the distribution of the 2145 MS-identified proteins from PICh according to their abundancy (sum intensity value). Some of known centromeric components (CENPs) are highlighted as red dots.

D. Volcano plot showing the regulated centromeric proteins identified by TMT-PICh performed in the indicated cell lines compared to WT control. Red, blue and green dots represent hits, candidates and no-hits proteins, respectively. Hits: false discovery rate (fdr) < 0.05 and fold change (FC) > 2; Candidates: fdr < 0.2 and a FC > 1.5.

E. Heat map showing the fold change ($\log_2$ ratio) of known centromeric and kinetochore proteins in the indicated conditions compared to WT.

F. Ontology analysis of the regulated centromeric proteins (n=594) identified by the PICh (hits + candidates).

G. Heat map showing selected centromeric proteins regulated among the indicated conditions identified by the PICh involved in DNA damage, DNA repair and replication. Categories were manually assigned based on the available literature. UFB: Ultra-Fine Bridges.

Figure 5. TOP2A, SMC5/6 and Translesion Synthesis Polymerases sustain centromere stability.

A. Schematic illustration of the experiments shown in B-D. IAA: Auxin; W/O: washout; DOX: Doxycycline.

B. (Left) Representative images of centromeric FISH on chromosome spreads from P/A in treated HCT116 cells with IAA (9-13 h from Palbociclib release). The fractions of analyzed metaphases showing 0, 1 and ≥ 2 centromere breaks are represented. Arrow indicates the presence of centromeric breaks. Scale bar = 5 μm. (Right) Centromeric breaks quantification per observed metaphase in the indicated conditions. N = 7, n = 28-63 analyzed metaphases/experiment (table S3). Error bars represent the standard error of the mean (SEM). χ^2 test (breaks vs non-breaks) ****p < 0.0001.

C. (Left) Representative immunofluorescence image and (right) relative quantification of centromeric 53BP1 after TOP2A and SMC6 IAA-induced depletion. Each dot represents one experiment depicted with a different shape (n = 80-472 analyzed cells/experiment, table S3). The bars represent the SEM. χ^2 test (breaks vs non-breaks) ****p < 0.0001.

D. (Left) Representative images of centromeric FISH on chromosome spreads from P/A treated HCT116 cells with IAA. The fractions of analyzed metaphases showing 0, 1 and ≥2 centromere breaks are represented. Arrow indicates the presence of centromeric breaks. Scale bar = 3 μm. (Right) Centromeric breaks quantification per observed metaphase in the indicated conditions. N = 4, n = 35-70 analyzed metaphases/experiment (table S3). Error bars represent the standard error of the mean (SEM). χ^2 test (breaks vs non-breaks) ****p < 0.0001.

E. Replication fork velocity quantification measured at centromere and bulk DNA in untreated and doxycycline-induced REV3L depleted RPE-1 after release (10 h) from G1 arrest by Palbociclib. n=80-184 analyzed DNA fibers per condition (table S3). Dark bars indicate the median, dashed lines the interquartiles. Mann–Whitney U test: *p = 0.0163.

F. Quantification of the number of ongoing forks per 100 kb centromeric fiber length in untreated and doxycycline-induced REV3L depleted RPE-1 after release (10 h) from G1 arrest by Palbociclib. n=172-196 analyzed DNA fibers per condition (table S3). Dark bars indicate the median, dashed lines the interquartiles. Mann–Whitney U test: *p = 0.0327.

G. Quantification of centromeric 53BP1 foci after REV3L doxycycline-induced depletion or JH-RE-06-mediated inhibition (1.5 or 3 μM). Each dot represents one experiment depicted with a different shape (n = 91-235 analyzed cells/experiment, see table S3). The bars represent the SEM. χ^2 test (breaks vs non-breaks) **p = 0.0057, ****p < 0.0001.

H. (Left) Representative images of centromeric FISH on chromosome spreads from P/A treated RPE-1 cells with DOX (24 h) to induce REV3L depletion. The fractions of analyzed metaphases showing 0, 1 and ≥2 centromere breaks are represented. Arrow indicates the presence of centromeric breaks. Scale bar = 5 μm. (Right) Centromeric breaks quantification per observed metaphase in the indicated conditions. N = 3, n = 31-84 analyzed metaphases/experiment (table S3). Error bars represent the standard error of the mean (SEM). χ2 test (breaks vs non-breaks) *p = 0.0405, **p = 0.0024.

I. Violin plot showing quantification of centromeric γH2A.X signal intensity in RPE-1 cells treated as shown in Figure 2I to achieve MiDAS inhibition. TLS inhibition was performed by JH-RE-06 treatment (3 μM) for whole duration of the experiment. Dots depicted with different shapes represent the mean value of one experiment. Dark bars indicate the median, dashed lines the interquartiles. N = 3, n =25-56 analyzed cells/experiment (table S3). Unpaired t-test p* = 0.0175, 0.0171; **p = 0.0067; **** p < 0.0001.

Figure 6. Tumors exhibit frequent centromere alterations, which result from prolonged replication stress.

A. Examples of heatmaps of copy number segments in colon adenocarcinoma (COAD) tumor samples from TGCA dataset. The colors represent the copy number categories of each segment (measured via the formula: Val = $2\log_2$ (total Copy Number/Ploidy) * 2). The dashed horizontal line indicates the centromere, and each column on the x-axis represents a sample. Only samples with > 0.7 purity were included in this analysis.

B. Boxplots showing the percentage of copy number alterations (CNAs) with breakpoints in centromeric regions (± 50 kbp) across the TCGA pan-cancers dataset. Data points represent individual cancer samples. Cancer cohorts are ordered by their median fraction of CNAs with centromeric breakpoints. Boxplots indicate first quartiles, medians (horizontal line) and third quartiles. Whiskers indicate minima and maxima within 1.5 inter-quartile range from the first and third quartiles, respectively. Cancer cohort abbreviations are explained in Table S4.

C. Bar graph showing the percentage of breaks occurring in the peri/centromeres (± 5 Mb) out of total breaks in 31 ovarian cancer models (OCM). High-grade serous ovarian cancers (HGSOC) are shown in red, low-grade serous ovarian cancers (LGSOC) in blue and mucinous in green. Datasets are ordered by their number of total detected breaks (grey triangle).

D. Scatter plot showing centromeric breaks enrichment over p-value for all chromosomes (indicated by their relative number). Enrichment of 1 (no more or less than expected) is indicated by the red dashed line.

E. Example of breakpoints enrichment on chromosome 5, 19 and 20 from pseudo-bulk single-cell WGS. Each red dot represents the center-point of an assayed window. Y-axis shows the enrichment score of the number of breakpoints occurring in each window, based on the expected number of breakpoints in a window the size of that chromosome's centromere. Enrichment of 1 (no more or less than expected) is indicated by the red dashed line. Blue box indicates the location of the centromere and the black line indicates the start and the end of the chromosome.

F. Representative images of WACT or aneuploidy in OCMs from patients #2, #5 (both LGSOC) and #24 (HGSOC) visualized by mFISH followed by a centromeric FISH (CENP-B box probe in green).

G. Scatter plot of number of WACT for cells in OCMs from 3 different patients (stroma (S) or tumour (T) cells). n = 20 analyzed metaphases/experiment (table S3). Unpaired t-test ***p = 0.0002; ****p < 0.0001.

H. Bar plot showing the coefficient of variation (difference of minimum and max intensity expressed as %) of α-satellite signal measured in WT and p53 shRNA RPE-1 cells treated as indicated. Error bars represent the SEM. N = 2, n = 20 analyzed cells/experiment (table S3). Unpaired t-test *p = 0.0246; **p = 0.0050, 0.0008.

I. Percentage of metaphases quantification showing centromeric/non-centromeric rearrangements in WT and p53 shRNA RPE-1 cells treated as indicated (APH 2 days: 200 nM + Cdc7i: 10μM; 8 and 16 days: 100 nM). Error bars represent the SEM. N = 3, n = 20 analyzed cells/experiment (table S3). Unpaired t-test **p = 0.0091; ***p = 0.0064.0064.

J. Quantification of the frequency (%) of the indicated chromosomal aneuploidies compared to diploid karyotype in WT and p53 shRNA RPE-1 cells treated as indicated (APH 2 days: 200 nM + Cdc7i: 10μM; 8 and 16 days: 100 nM). N = 22, n = 20 analyzed cells/experiment.

Figure 7. Model of centromere DNA replication and stability.

Human centromeres harbour a specialized DNA replication program. Alteration of this program causes replication stress and centromere breakage in mitosis, leading to recombination and defective repair, whole-arm chromosome translocation and aneuploidy.

STAR★METHODS

Key resources table

REAGENT or RESOURCE	SOURCE	IDENTIFIER
Antibodies		
Avidin FITC	Thermo Fisher	Cat# 434411
Rabbit Anti Avidin biotin conjugated	Rockland laboratories	Cat# 200-4697-0100 RRID:AB_2612523
rat anti-BrdU	Abcam	Cat# ab6326 RRID:AB_305426
mouse anti-BrdU	BD Bioscience	Cat# 347580 RRID:AB_10015219
goat anti-mouse Cy5.5	Abcam	Cat# ab6947 RRID:AB_955087
donkey anti-goat Cy5.5	Abcam	Cat# ab6951 RRID:AB_955084
donkey anti-rat 594	Jackson laboratory	Cat# 712-585-150 RRID:AB_2340688
rabbit single-stranded DNA	Tecan, IBL international	Cat# JP 18731 RRID:AB_2341405
Anti-Centromere Antibody (ACA)	Antibodies Incorporated	Cat# 15-235-0001 RRID: AB_2797146
Rabbit polyclonal 53BP1	Novus-biologicals	Cat# NB100-304 RRID:AB_10003037
γH2AX	Millipore	Cat# 05-636 RRID:AB_309864
γH2AX	Cell Signaling	Cat#9718 RRID:AB_2118009
CENP-C	MBL	Cat# PD030 RRID:AB_10693556
MUS81	Santa Cruz	Cat# SC-53382 RRID:AB_2147138

Donkey polyclonal anti-guinea pig - Alexa Fluor 647	Jackson ImmunoResearch Laboratories	Cat# 706-605-148; RRID: AB_2340476
Donkey polyclonal anti-mouse - Alexa Fluor 488	Jackson ImmunoResearch Laboratories	Cat# 715-545-150; RRID: AB_2340846
Donkey polyclonal anti-rabbit - Cy3	Jackson ImmunoResearch Laboratories	Cat# 711-165-152; RRID: AB_2307443
Azide-Alexa Fluor 488	Invitrogen	Cat #A10266
Azide- Alexa Fluor 647	Invitrogen	Cat #A10277
CENP-B	Abcam	Cat# ab25734 RRID:AB_726801
mini-AID tag	MBL	Cat# M214-3 RRID:AB_2890014
GAPDH	Cell Signaling	Cat# 2118
VINCULIN	Sigma	Cat# V9264 RRID:AB_10603627
CENPA	Cell Signalling	Cat# 2186 RRID:AB_561053
CENP-B	Abcam	Cat# 259855 RRID: AB_3075448
CENP-C	Milllipore	Cat# ABE1957 RRID: AB_3075449
FLAG	Sigma-Aldrich	Cat#F3165 RRID:AB_259529
Chemicals, peptides, and recombinant proteins		
Palbociclib	Sigma-Aldrich	Cat# PZ0383
Aphidicolin	Sigma Aldrich	Cat# A0781
JH-RE-06	Glixxolabs	Cat# GLXC-21219
Hydroxyurea	Sigma Aldrich	Cat #H8627
VE-821	Sigma Aldrich	Cat #SML1415
XL413	Tocris	Cat# 5493
Olaparib (PARPi)	Sigma Aldrich	Cat# AZD2641
IFN-ß	PeproTech	Cat# 300-02BC
Calyculin A	Sigma Aldrich	Cat# C5552
Indole-3-Acetic Acid	Sigma Aldrich	Cat# I5148
5-Phenyl-1H-indole-3-acetic acid	Sigma Aldrich	Cat# SML3574
Doxycycline	Sigma Aldrich	Cat# D2507
Polybrene	Santa Cruz	Cat# 28728-55-4
Puromycin	Gibco	Cat# A1113803
esiRNA MUS81	Sigma Aldrich	Cat# EHU020611
esiRNA control	Sigma Aldrich	Cat# EHURLUC
Lipofectamine RNAiMAX Transfection Reagent	Thermo Fisher	Cat# 13778075
OptiMEM	Thermo Fisher	Cat# 31985062

Quick-RNA Miniprep Plus	Zymo Research	Cat# R1057
SuperScript™ III Reverse Transcriptase kit	Thermo Fisher	Cat# 18080093
LightCycler 480 SYBR Green I Master	Roche	Cat# 04707516001
proTAME	R&D systems	Cat# I-440
Apcin	Sigma Aldrich	Cat# SML1503
Nocodazole	Sigma Aldrich	Cat# M1404
KCl	Thermo Fisher	Cat# 15691160
RO-3306	Enzo	Cat# ALX-270-463
Acetic acid	Sigma Aldrich	Cat# 33209-M
Dextran	MERCK	Cat# 31389
Formamide	Sigma Aldrich	Cat# 47671
SSC	Euromedex	Cat# EU0300
Human Cot1	Roche	Cat# 11581074001
Salmon sperm	Thermo Fisher	Cat# 15632011
EtOH	VWR	Cat# 20821310
Chloroform	VWR	Cat# 200-663-8
ProLong Gold antifade reagent with DAPI	Invitrogen	Cat# P36935
Colcemid	Sigma-Aldrich	Cat#vD1925
EDTA	Invitrogen	Cat# 15575-020
IdU	Sigma-Aldrich	Cat# 7125
CldU	Sigma-Aldrich	Cat# 6891
Thymidine	Sigma-Aldrich	Cat# 1895
Low melting agarose	Sigma Aldrich	Cat# 4018
Proteinase K	Roche	Cat# 3115844001
β-agarase	NEB	Cat# M0392L
MES	Merck	Cat# 69889
Engraved Combicoverslips	Genomic Vision	Cat# COV-002-RUO
NaOH	VWR	Cat# 28224296
Blocking aid	Roche	Cat# 11096176001
NaCl	GE healthcare	Cat# 17-5175-01
ProLong Gold antifade reagent	Invitrogen	Cat# P36935
Poly-L-lysine-coated coverslips	Fisher Scientific	Cat# BR475505
EdU	Sigma Aldrich	Cat# 900584
Cavity slides (Sigma-Aldrich, BR475505	Sigma-Aldrich	Cat# BR475505
$CuSO_4$	Jena Bioscience	Cat# CLK-MI004
Na-Ascorbate	Jena Bioscience	Cat# CLK-MI005
Propidium iodide	Thermo Fisher	Cat# P3566
RNAseA	Sigma	Cat# R5000
Hoechst	Invitrogen	Cat# 33258
Exonuclease III	Promega	Cat# M1811
DAPI	Sigma Aldrich	Cat# 28718-90-3
Pierce High Capacity Streptavidin Agarose	Thermo Fisher	Cat# 20361
Pierce Centrifuge Columns	Thermo Fisher	Cat# 89898
Dynabeads™ MyOne™ Streptavidin C1	Thermo Fisher	Cat# 65002
D-Biotin	Thermo Fisher	Cat# B20656
Sephacryl S-400 HR	Thermo Fisher	Cat# GE17-0609-10

Trichloroacetic acid solution	Thermo Fisher	Cat# T0699
SilverQuest ™ Silver Staining Kit	Thermo Fisher	Cat# LC6070
Sera-Mag SP3 SpeedBeads	GE Healthcare	Cat# 45152105050250
TMTsixplex	Thermo Fisher	Cat# 90061
Experimental models: Cell lines		
hTERT RPE-1	ATCC	RRID: CVCL4388
HCT116	ATCC	RRID: CVCL0291
TOP2-mAC HCT116	Yesbolatova et al. [73]	N/A
Tet-OsTIR1 SMC6-mAID-Clover HCT-116	Venegas et al. [69]	N/A
hTERT RPE-1 CENP-A EYFP-AID	Hoffmann et al. [53]	N/A
hTERT RPE-1 CENP-A EYFP-AID; CENP-B -/-	Hoffmann et al. [53]	N/A
hTERT RPE-1 *CENP-B* $^{-/-}$	Hoffmann et al. [53]	N/A
hTERT RPE-1 LT3GEPIR REV3L	This paper	N/A
hTERT RPE-1 CENPB DBD-FLAG-ETAA1 AAD-FLAG	This paper	N/A
hTERT RPE-1 Neo4p13	Murillo-Pineda et al.[42]	N/A
Recombinant DNA		
LT3GEPIR_REV3L	This paper	N/A
pINDUCER 20_CENPB DBD-FLAG-ETAA1 AAD-FLAG	This paper	N/A
Other		
CENP-B Box Cy3 FISH probe	PNA Bio	Cat# F3002
FRA3B FISH probe	Gift from B. Le Tallec	N/A
FRA4B FISH probe	Gift from B. Le Tallec	N/A
six ~ 50 bp each 2'F-RNA biotinylated probes	Giunta Hervé et al.[11]	N/A
24XCyte Human Multicolor FISH Probe	MetaSystems Probes	Cat# D-0125-060-DI
CENP-B Box Alexa488 FISH probe	PNA Bio	Cat# F3004
CENP-B-RC-Cy3 FISH probe	PNA Bio	Cat# F3009
Software and algorithms		
Fiji	http://fiji.sc	RRID:SCR_002285
Metafer	Metasystem	RRID:SCR_016306
FlowJo	BD	RRID:SCR_008520
Neo--Acquisition software	Abbelight	N/A
Matlab	Mathworks	RRID:SCR_001622
R Project for Statistical Computing	Dessau et al [104]	RRID:SCR_001905
Jamovi	www.jamovi.org	RRID:SCR_016142
GraphPAD Prism v9	GraphPad Software	RRID:SCR_002798
Aneufinder v1.26.0	Bakker et al [86]	N/A
Isobar quant	Breitwieser et al [105]	N/A
Mascot	Matrix Science	RRID:SCR_014322
Limma	Ritchie et al. [106]	RRID:SCR_010943
Metascape	www.metascape.org	RRID:SCR_016620
Deposited data		

Immunoblots and Immunofluorescence raw data	This study	Mendeley dataset 10.17632/bjtcdm6zm8.1
scWGS karyotyping data from OCMs	Coulson-Gilmer et al.[80] Nelson et al. [81]	PRJEB47696 PRJEB28664
Proteomics raw data	This study	PRIDE database[107] PXD047847

RESOURCE AVAILABILITY

Lead contact

Further information and requests for resources and reagents should be directed to and will be fulfilled by the Lead Contact, Daniele Fachinetti (daniele.fachinetti@curie.fr).

Materials availability

Plasmids and cell lines generated in this study will be provided upon request to the Lead Contact.

Data and code availability

- All raw data for TMT-PiCh Mass Spectrometry have been deposited at PRIDE - Proteomics Identification Database (EMBL-EBI) under the accession number PXD047847 and are publicly available. scWGS karyotyping data from OCMs are from datasets published elsewhere[80,81] and raw data have been deposited at EMBL-EBI under the accession number PRJEB47696 and PRJEB28664; the FASTQ files are available from the European Nucleotide Archive. Raw data of main images and immunoblots have been deposited on Mendeley 10.17632/bjtcdm6zm8.1. All accession numbers are listed in the key resources table. All other data reported in this paper will be shared by the lead contact upon request.
- This paper does not report original code.
- Any additional information required to reanalyze the data reported in this paper is available from the Lead Contact upon request.

Experimental model and study participant details

Cell lines

Immortalized hTERT retinal pigmented epithelial (RPE-1) cells were grown in Dulbecco Modified Minimal Essential medium DMEM:F-12 (Life Technologies) supplemented with 10 % fetal bovine serum (FBS), or 10% tetracycline-free FBS (Atlanta Biologicals), 100 U/LmL Penicillin-Streptomycin (Life Technologies), 0.1% sodium bicarbonate and 2 mM L-glutamine.

Colorectal cancer HCT116 cell lines (ATCC, RRID: CVCL0291) were maintained in McCoy (Life Technologies) supplemented with 10 % fetal bovine serum (FBS), or 10 % tetracycline-free FBS (Atlanta Biologicals), 100 U/LmL Penicillin-Streptomycin (Life Technologies) and 2 mM L-glutamine.

Patient samples

Research samples for the ovarian cancer models were obtained with informed patient consent from the Manchester Cancer Research Centre (MCRC) Biobank. The MCRC Biobank is licensed by the Human Tissue Authority (license number: 30004) and is ethically approved as a research tissue bank by the South Manchester Research Ethics Committee (Ref: 18/NW/0092).

Method details

Cell Culture and treatments

Cell cycle synchronization was obtained by treatment with 0.5 (RPE-1, ATCC, RRID: CVCL4388) or 1 µg/mL (HCT116) Palbociclib (Sigma Aldrich, PZ0383) for 24 h. Palbociclib removal (washout) was performed by four washes in complete medium. For time-course experiments, cells were released from 24h Palbociclib treatment in presence or not of APH (200 nM) and fixed at different time-points. To compare cells in the same cell cycle phase upon different treatments, the following conditions were compared: G1: 3 h NT, 3 h APH; S: 8 h NT, 12 h APH; G2: 12 h NT, 24 h; second G1 (under a second Palbociclib block): 30 h NT, 30 h APH.

Treatments with the following chemicals were performed as indicated throughout the text: Aphidicolin (100 or 200 nM; Sigma Aldrich, A0781), JH-RE-06 (REV3Li) (1.5 or 3 µM; Glixxolabs, GLXC-21219), Hydroxyurea (HU) (0.5 mM), XL413 (Cdc7i) (10 µM; Tocris 5493), Olaparib (PARPi) (5 µM; Sigma Aldrich, AZD2641), IFN-ß (30 U/mL; PeproTech, 300-02BC), Calyculin A (50 ng/mL; Sigma Aldrich, C5552), ATRi (VE-821) (10 µM; Sigma-Aldrich), CDK1 inhibitor (R0 3306) (7.5 µM, Enzo, Cat# ALX-270-463), Indole-3-Acetic Acid (IAA; 500 µM; Sigma Aldrich , I5148), 5-Phenyl-1H-indole-3-acetic acid (1 µM; a gift from Kanemaki's lab) and Doxycycline (Dox, 100 ng/mL).

Plasmids Generation

To generate LT3GEPIR plasmids, targeting sequences against the genes of interest were selected from[108], and cloned accordingly to authors 'instructions into LT3GEPIR empty vector (Addgene #111177).

REV3L oligomer sequence is: 5`-TGCTGTTGACAGTGAGCGAAAGGATGTTCACTGTCTGTTATAGTGAAGCCACAGATGTATAACAGACAGTGAACATCCTTGTGCCTACTGCCTCGGA-3`.

Doxycycline-inducible ETAA1 ATR activator domain (ETAA1 AAD) vector was generated by fusing the coding sequence of the ETAA1 protein domain corresponding to 56-220 AA (kind gift of Vincenzo Costanzo, IFOM, Milan) in frame with the CENP-B DNA binding domain (DBD), FLAG and microAID sequence. eGFP sequence was also cloned after a tPT2A sequence. Amplicons were generated by PCR, assembled by the Gibson method and cloned into a pDEST shuttle vector. Gateway cloning was employed to transfer the coding sequence into a pInducer 20 backbone (Addgene #44012) by LR II recombinase (Invitrogen, cat. 11791020).

Cell lines Generation

Doxycycline-inducible miR-E shRNA and ETAA1 AAD-CENP-B DBD-AID cell lines were generated by transduction with lentiviral particles delivering LT3GEPIR and pINDUCER 20 vectors, respectively, for 16 h in presence of 8 µg/mL polybrene. Cells were then selected by puromycin (2 µg/mL, LT3GEPIR) or G418 (0.5 mg/mL, pINDUCER) and induced with doxycycline (1 µg/mL LT3GEPIR; 0.1 µg/mL, pINDUCER) for the indicated time.

Endoribonuclease-prepared siRNA targeting MUS81 (esiRNA Sigma-Aldrich, EHU020611) were transfected twice with a 24h interval into cells with Lipofectamine RNAiMAX Transfection Reagent (Thermo Fisher) at 0.35 µg/mL final concentration mixed in serum-free medium OptiMEM (Thermo Fisher). Cells were analyzed 72h post-transfection.

RNA extraction, Reverse Transcription and RT-qPCR

Total RNA was extracted with the Quick-RNA Miniprep Plus (Zymo Research, R1057) and retro-transcribed with SuperScript™ III Reverse Transcriptase kit (Thermo Fisher 18080093) according to the manufacturer's instructions. Real-time quantitative PCR (RT-qPCR) was carried out using LightCycler 480 SYBR Green I Master (Roche) and appropriate primer sets, previously tested for amplification efficiency. Primers are listed below:

Gene	Sequence 5`- 3'
REV3L	FW_TGTGAAAAACCGTCTCAGCG REV_CACGGACGCAACCACTCG
GAPDH	FW_GTCTCCTCTGACTTCAACAGCG REV_ACCACCCTGTTGCTGTAGCCAA
ISG15	FW_GTGGACAAATGCGACGAACC REV__TCGAAGGTCAGCCAGAACAG

Fluorescence *in situ* hybridization (FISH)

Cells were blocked in mitosis without or with 3 to 4 hr of 12.5 µM proTAME (R&D systems, I-440) and 25 µM Apcin (Sigma, SML1503**)** (P/A) or 3hr Nocodazole (10 ng/mL). Cells were harvested and swollen in hypotonic solution (75 mM KCl) and fixed with acetic acid/ethanol (1:3) and spread onto slides. Coverslips were rinsed with 80% ethanol and air dried.

For CENP-B box FISH: CENP-B boxes Cy3 probe (PNA Bio) diluted in hybridization buffer (10% Dextran, 50% Formamide in 2x SSC, 1% Tween) (1/300) probe was applied. Probe and sample were denatured by heating (65°C, 2 min) followed by a 2h incubation at 37°C. Then slides were washed with 0.4X SSC at 72°C for 2 min, washed in 2X SCC, 0.05% Tween 20 at RT for 30 sec.

For FISH on CFS FRA3B or FRA4B: for one sample 150 ng of biotinylated probe in combination with 10 µM of human Cot1 DNA from Roche and 5 µM of salmon sperm was precipitated overnight with 1/10 volume Sodium Acetate 3M pH 5.5 and 2.5 volumes of cold EtOH 100%.

Probes were pelleted, air dried and resuspended in 5 µl of TE 1X. Probe denaturation was performed by adding 22.5 µL of hybridization buffer prewarmed at 37°C, incubation for 20 min at 37°C, 5 min at 75°C, fast cooling on ice and reannealing at 37°C for 20 min. Slides were treated with 100 µg/µL RNase A in 2X SSC for 1h at 37°C. Slides were dehydrated by multiple immersions in increasing concentrations of EtOH 70, 85, 100% for 5 min RT. Slides were denatured with 70% formamide in 2X SSC at 72°C for 2 min on a hot plate. After denaturation, slides were dehydrated with EtOH cooled at 4°C. Probe was incubated at 37°C overnight in a humified chamber.

After hybridization, coverslips were removed and slides were washed 5 times for 5 min in 50% formamide/2X SSC pH 5.6 at 45°C, 5 times for 5 min in 2X SSC at 45°C and 5 min in 4X SSC 0.05% Tween-20 at RT.

All slides were rinsed with PBS, mounted in ProLong Gold antifade reagent with DAPI (Invitrogen, P36935) and imaged with an epifluorescence microscope (Leica DM6000), 100X objective.

Multicolor-FISH Karyotyping and Sequential FISH

OCMs and associated patient-derived stromal cell cultures were grown to 80% confluency in T75 flasks, then incubated in 100 ng/MmM Colcemid for 4 hr (stromal cells) or 6 hr (OCMs).

RPE-1 cells ±APH were instead treated with P/A for 3 hr. Cells were then collected and centrifuged at 1200 rpm for 10 mins, before addition of 75 mM KCL and incubation at RT for 10 mins, then 20 mins on ice. Cells were pelleted, then incubated in Carnoy's fixative at RT for 30 mins, before being pelleted and suspended in further Carnoy's fixative and stored at -20°C.

Cells were then prepared as described in Trott et al.[109] for the mFISH karyotyping. Briefly, cells were dropped onto glass slides and air dried. mFISH was performed according to manufacturer's protocol (MetaSystem). The Metafer imaging platform (MetaSystems) and the Isis software were used for automated acquisition of the chromosome spread and mFISH image analysis.

In order to combine mFISH karyotyping and FISH using alpha satellite probe to localize the centromere, the first mFISH hybridization was stripped. After coverslip removal, the slide was washed in EtOH 70% for 1 min. Prewarmed denaturation solution (70% formamide, 2X SSC, pH 7.0) was applied and the slide was placed on a hotplate at 75°C for 2 min. The slide was then washed in 70% EtOH for 1 min and subsequently dehydrated in 90% and 100% EtOH for 1 min. The sample was air-dried and hybridization with the new probe was performed.

The intensity of alpha satellite signal was measured using Fiji. For each spread, every visible alpha satellite was quantified and then normalized to the mean of all centromeric intensities calculated on the values falling in the range between the 25-75% percentiles. The normalized values of each spread were then grouped for every individual chromosome and experimental conditions; a second normalization was then performed for each experimental condition to the untreated to normalize for chromosome-specific alpha satellite variations. For all the metaphase spreads, the number of gain and losses for every chromosome was also calculated. To determine the aneuploidy score, the number of gain and losses was divided by the number of spreads analyzed in each replica and reported as percentage. The value plot in the heatmap is the final percentage mean between all replicas.

Breakpoint hotspot analysis

To investigate the presence of centromere instability in human cancers, we used the absolute copy number data generated by Steele et al. (2022)[78] from the TCGA consortium cohort. Only samples with tumour purity greater than 70% were included in this analysis to reduce the confounding effects from stromal/normal contamination, resulting in a total of 2897 individual tumour samples from 33 different cancer types. Centromeric aneuploidy events at the sample level were counted as number of non-neutral copy number segments with at least one breakpoint overlapping with the centromeric regions (+/- 50 kbp). The resulting values were normalised by the total number of non-neutral copy number events in each sample.

For the ovarian cancer models, research samples were obtained with informed patient consent from the Manchester Cancer Research Centre (MCRC) Biobank. The MCRC Biobank is licensed by the Human Tissue Authority (license number: 30004) and is ethically approved as a research tissue bank by the South Manchester Research Ethics Committee (Ref: 18/NW/0092). The role of the MCRC Biobank is to distribute samples and does not endorse studies performed or the interpretation of results. For more information, see https://www.mcrc.manchester.ac.uk/research/mcrc-biobank.

Derivation of ovarian cancer models, culture and single-cell WGS for the samples used in this analysis has been reported previously[79-81]. To ensure that clonally-related breakpoints are not represented by multiple different breakpoints called in individual cells, aligned sequencing reads for single cells in bam format were merged using SAMtools. AneuFinder (v 1.26.0) was then used to call copy number states and breakpoints on the pseudo-bulked samples, with 'refine.breakpoints' set to true and binsize set to 1mb.

Peri/centromere breaks in each ovarian cancer model were determined as the intersection of the refined breakpoints from AneuFinder and the centromere coordinates as given by the UCSC Table Browser +/- 5 Mb (to include the pericentromeric regions)[5]. For each ovarian cancer model, this was expressed as a proportion of the total number of breaks occurring not in the peri/centromere regions.

To determine whether breakpoints were enriched in centromeres, we created sliding windows of the width of the centromere for each chromosome, which were staggered by 50 kb. The breakpoints falling into each bin were summed, and enrichment determined based on the number of breakpoints within each window versus the number of breakpoints expected in a window of that size based on the total number of breakpoints on that chromosome. Significance of enrichment was determined by Fishers exact test for each window. Whether breakpoints were enriched in centromeres was determined by a window with $p < 0.05$ overlapping with centromere coordinates as given by the UCSC genome browser.

DNA Combing

Cells were pulse-labeled with 20 min of 100 μM IdU (Sigma Aldrich, 7125) followed by 20 min of 100 μM CldU (Sigma Aldrich, 6891) and chased by 1 mM Thymidine for 5 min (Sigma Aldrich, 1895). Note that labeling was extended to 50 min for APH experiments and 30 min for dox-inducible shRNA REV3L cells for both IdU and CldU. Cells were harvested, embedded in 2% low melting agarose (Sigma Aldrich, 4018) and incubated overnight at 42°C in Proteinase K solution. Next day agarose blocks were treated with Protease inhibitor (Roche, 3115844001), washed several steps in TE buffer (10 mM Tris-HCl, 1 mM EDTA). Blocks were melted in β-agarase (NEB, M0392L) solution at 68°C for 15min, followed by overnight β-agarase treatment at 42°C. Melted agarose blocks were diluted in 0.25M MES solution and incubated for at least 1week before combing onto silanized coverslips (home-made according to[110] or Engraved Combicoverslips supplied by Genomic Vision #COV-002-RUO) with the FiberComb device (Genomic Vision) at a constant speed of 300 µm/sec.

DNA was denatured for 5 min in 1N NaOH, followed by PBS (4°C) wash and dehydration in increasing concentrations of EtOH (75, 80 and 100%). Slides were hybridized overnight at 37°C with biotinylated centromeric probes (see PICh section for details) and the next day washed (3X) with 50% formamide solution at RT. After 3 washes in 2X SSC and a quick wash in PBS, slides were incubated for 1h in blocking solution (Roche, 11096176001) at 37°C. Centromere signal was detected by alternating layers of Avidin FITC (1:100, Thermo Fisher #434411) and Rabbit Anti Avidin biotin conjugated (1:50, Rockland laboratories #200-4697-0100) and replication was detected with rat anti-BrdU (1:25, Abcam ab6326) and mouse anti-BrdU (1:5, BD Bioscience 347580) for 1 hr at 37°C. After a short wash step (0.5 M NaCl, 20 mM Tris, pH 7.8, and 0.5% Tween 20), the fibers were incubated with goat anti-mouse Cy5.5 (1:100, Abcam ab6947) donkey anti-goat Cy5.5 (1:100, Abcam ab6951) and donkey anti-rat 594 (1:50, Jackson laboratory #712-585-150) each for 20 min. For bulk genome inter-origin and inter termination distance, single stranded DNA was detected with rabbit single-stranded DNA antibody (IBL international, JP

18731) and replication was detected with goat anti-mouse Cy5.5 (1:100, Abcam ab6947) donkey anti-goat Cy5.5 (1:100, Abcam ab6951) and donkey anti-rat 594 (1:50, Jackson laboratory #712-585-150) each for 20 min. Fibers were mounted in ProLong Gold antifade reagent (Invitrogen P36935) and acquisition was performed with an epifluorescence microscope (40X, Apotome, Zeiss) with available mosaic option. Replication tracks were measured using FIJI software.

Immunofluorescence

Cells were grown on poly-L-lysine-coated coverslips and fixed in PBS containing 4% formaldehyde and 0.1% Triton X-100 at RT for 10 min. Blocking was performed with 5 % Bovine Serum Albumin in 0.1 % Tween-20 in PBS for 10 min or in 2.5 % FBS (v/v), 0.2 M glycine, 0.1 % triton X-100 (v/v) in PBS for 30 min at RT. Primary antibodies were incubated in blocking buffer for 1 hr at RT. After washing with PBS 0.1% Triton X-100, coverslips were incubated with secondary antibodies conjugated to fluorochromes (Jackson Immuno Research) for 45 min at RT. The following antibodies were used: 53BP1 (1:500, Novus Biologicals NB100-304), ACA (1:500, Antibodies Incorporated #15-235-0001), CENP-C (1:1000, MBL PD030), γH2A.X (1:200, Millipore #05-636; 1:1000, Cell Signalling #9718), FLAG (1:1000, Sigma-Aldrich F3165). Coverslips were mounted using anti-fade reagent Prolong Gold containing DAPI (Life Technologies). Images were acquired on a DeltaVision Core system (Applied Precision) with 60X Olympus UPlanSApo oil-immersion objective (NA 1.4), 250 W Xenon light source equipped with a Photometrics CoolSNAP_HQ2 Camera. 4 μm Z-stacks were acquired (Z step size: 0.2 μm).

Immunofluorescence of metaphase spreads

RPE-1 cells were grown to 80% confluency on coverslips and treated with either 12,5 μM proTAME and 25 μM Apcin or Nocodazole (10 ng/mL) for 3h. Cells were incubated with hypotonic medium (75 mM KCl) for 10 min at 37°C and then centrifuged at 1500 rpm for 8 min. Cells were fixed in 4% formaldehyde 0.1% Triton X-100 at RT for 10 min and subsequently incubated in a blocking buffer (2 % FBS in PBS) for 30 min at RT. Primary antibodies were incubated in blocking buffer for 1 hr at RT and used as follows: CENP-C (1:1000, MBL PD030), γH2A.X (1:1000, Abcam ab25734), MUS81 (1:200, Santa Cruz 53382). The following secondary antibodies were used (1:400): donkey anti-Guinea Pig Alexa Fluor 647, donkey anti-rabbit Cy3, donkey anti-mouse Alexa Fluor® 488. After immunostaining, cells were mounted using ProLong Gold antifade reagent with DAPI (P36935, Invitrogen).

Cen-CO-FISH

CO-FISH at centromere was performed as previously described[88]. Briefly, cells were grown in 6-well plates for 48 h in the presence of APH +/- the Cdc7 inhibitor XL413. 10 μM BrdU:BrdC (3:1) was added for 20-24h and ProTAME/Apcin (12.5 μM and 25 μM, respectively) 3 h before harvesting mitotic cells. Cells were collected by mitotic shake off in 2 mL 1X PBS, washed several times and pelleted by centrifugation and final suspension in 100 μL 1X PBS. 1 mL 0.56% KCl (hypotonic buffer) was added dropwise to the side of the tube, cells were incubated for 6 min at RT, spun down and the pellet was suspended in remaining liquid. 1 mM fixative (3:1 Methanol: Acetic Acid) was added dropwise and solution was incubated for 20 min at RT or 37° C, then centrifuged and washed again in fixative. After final centrifugation, all supernatant was removed, cells suspended in remaining fixative and spread onto coverslips. Coverslips were dried in absence of light. Slides were rehydrated in PBS for 5 min at RT, treated with 0.5 mg/mL RNase A (in PBS, DNase free) for 10 min at 37°C, stained with 0.5 µg/mL Hoechst 33258 (Sigma) in 2x SSC for 15 min at RT and the placed in a shallow plastic tray, covered by 2x SSC. Slides were exposed to 365 nm UV light at RT (Stratalinker 1800 UV irradiator) for 5.4×10^3 J/m^2. BrdU/BrdC-substituted DNA strands were digested with 80 µL of 10 U/µL of Exonuclease III (Promega) in buffer supplied by the manufacturer (50 mM Tris-HCl, 5 mM MgCl2, and 5 mM DTT, pH 8.0) at 37°C for 30 min, washed in PBS and dehydrated in ethanol series (5 min in 70%, 95%, 100% at RT) and air dried. For probe hybridization 100 µL hybridization solution was added at RT onto slides. After 30 min slides were hybridized for 1.5– 2 hours with 100 µL CENPB-RC-CY3 probe (1:200, PNA Bio F3009), at RT, in the dark humid chamber. Slides were rinsed in hybridization wash (10 mM Tris-HCl pH 7.2, 70% formamide, 0.1% BSA) for 2-5 seconds and hybridized for 1.5– 2 hours with 100 µL CENPB-Alexa488 probe (1:200, PNA Bio F3004), at RT in the dark humid chamber. Then, slides were washed again in hybridization wash for 15 min on shaker, following another wash in 0.1 M Tris-HCl pH 7.2, 0.15 M NaCl, 0.08% Tween-20 buffer 3 times for 5 min on shaker. After DAPI incubation, slides were dehydrated in ethanol series as above, air-dried, and mounted using ProLong Gold (Invitrogen), sealed with nail polish, stored at -20°C protected from light. Imaging was performed with Olympus FV1200 live cell confocal microscope with 100X magnification. Mitotic cells were detected by DAPI signal.

Centromeric EdU staining and cell cycle analysis

For EdU colocalization at centromere, cells were pulsed 10 min with EdU (10 µM final; Sigma Aldrich #900584,), fixed in 4% formaldehyde, permeabilized and click-labelled with homemade click chemistry buffer (Tris-HCl 100 mM, pH 8.5, $CuSO_4$ 1 mM, Azide-fluor 488 5 µM, Ascorbic acid 100 mM) for 30 min at RT. After washing with PBS 0.1% Triton X-100, coverslips were saturated in blocking buffer for 30 min and incubated with CENP-B antibody (1:500, Abcam ab25734) for 1h at RT. After washing with PBS 0.1% Triton X-100, coverslips were incubated with appropriate secondary antibody conjugated to fluorochrome and mounted with anti-fade Prolong Gold containing DAPI (Life Technologies). CENP-B / EdU colocalization was scored by in-house developed macro using Fiji software.

Detection of ssDNA was performed as in [111]. Cells were incubated with 10μM BrdU for 24h. At the end of the incubation, cells were treated with 0.5 M HU for two hours and 20 min before fixation cells were pulsed with 10 μM EdU. DNA denaturation was omitted, and cells were fixed and stained according to the published procedure[111]. Briefly, cells were washed in ice-cold PBS and incubated with pre-extraction buffer (25 mM Hepes pH 7.5, 50 mM NaCl, 1 mM EDTA, 3 mM $MgCl_2$, 300 mM sucrose, 0,5 % TritonX-100) for 5 min over ice. After washing, cells were fixed in ice-cold 4% paraformaldehyde for 10 min, saturated in 5% BSA for 1 h and click-labelled with homemade click chemistry buffer (Tris-HCl 100 mM pH 8.5, $CuSO_4$ 1 mM, Azide-fluor 647 5 μM, Ascorbic acid 100 mM) for 30 min at RT. After washing, cells were incubated with CENP-C (1:1000, MBL PD030) and BrdU antibodies (1:300, BD Bioscience 347580) diluted in 2.5 % BSA/PBS solution. Then cells were washed and incubated with secondary antibodies donkey anti-Guinea Pig Alexa Fluor Cy3, donkey anti-mouse Alexa Fluor 488. After immunostaining, cells were mounted using ProLong Gold antifade reagent with DAPI (Invitrogen, P36935).

For cell cycle analysis, growth medium was supplemented with 10 μM BrdU for 30 min before collection and fixation in 70% EtOH. Staining was performed using anti-BrdU antibody (1:25, BD 347580) followed by appropriate secondary antibody incubation. Finally, propidium iodide (Thermo Fisher) wad added at 2.5 μg/mL final concentration in presence of 250 μg/mL RNAse A

(Thermo Fisher) and incubated at least 1hr before acquisition on a LSRII Flow Cytometer (BD). Data were analyzed using FlowJo software v10 (BD).

Immunoblotting

Whole cell extracts were obtained by denaturation and sonication in SDS lysis buffer (200 mM TRIS pH 8.8, 4% SDS, 10% glycerol). Lysates were quantified by BCA method (Thermo Fisher), diluted in Laemmli Sample Buffer and incubated at 95°C for 5 minutes before being resolved by SDS-PAGE, transferred to nitrocellulose membranes and blotted with the following antibodies: MUS81 (1:500, Santa Cruz SC-53382), mini-AID tag (1:1000, MBL #M214-3), GAPDH (1:5000, Cell Signaling #2118), VINCULIN (1:5000, Sigma V9264).

Proteomics of Isolated Chromatin (PICh)

PICh was performed on the indicated cell lines as previously described[52,112] in triplicate, with adaptations. Briefly, c.a. 10^9 cells/condition were fixed in 3.7% formaldehyde for 45 minutes at RT; chromatin was extracted and sonicated with a microtip, pre-cleared with anti-streptavidin agarose beads (Invitrogen) and hybridized with an equimolar mix of six ~ 50 bp each 2'F-RNA biotinylated oligos (synthetized at W.M. Keck Biotechnology Resource Lab at Yale University). These probes, covering a 321 bp region, match the consensus sequence of 21 Higher Order Repeats families, distributed across all human centromeres bearing CENP-A binding. Sequences were published in *Giunta, Herve et al* (2021)[11]. Chromatin was recovered by MyOne Streptavidin dynabeads (Invitrogen), subjected to stringent washes, and eluted from beads by competition with D-Biotin (Invitrogen). Proteins from eluates were precipitated with Trichloroacetic Acid (TCA, Sigma-Aldrich) and decrosslinked at 99°C for 5 mins. Input and 1/10 of the eluted material were resolved on a 4-15% gradient polyacrylamide gel (Invitrogen) followed by Silver Staining and by immunoblot with the following antibodies: CENPA (1:1000, Cell Signalling #2186), CENP-B (1:1000, Abcam 259855), CENP-C (1:1000, Millipore ABE1957). Protein content was analyzed by quantitative Tandem Mass Tag LC Mass spectrometry as follows below.

Mass Spectrometry sample preparation and LC-MS/MS acquisition

Disulphide bridges in cysteine containing proteins were reduced with dithiothreitol (56°C, 30 min, 10 mM in 50 mM HEPES, pH 8.5), which were then alkylated with 2-chloroacetamide (room temperature, in the dark, 30 min, 20 mM in 50 mM HEPES, pH 8.5). Samples were purified by SP3 protocol[113,114] and trypsinized (sequencing grade, Promega) in an enzyme:protein ratio 1:50 overnight at 37°C. Peptides were recovered in two sequential elution in HEPES buffer from supernatant upon magnetic beads separation.

Peptides were labelled with TMT6plex[115] Isobaric Label Reagent (ThermoFisher) according to the manufacturer's instructions. Samples were combined for the TMT4plex and for further sample clean up an OASIS® HLB µElution Plate (Waters) was used. Offline high pH reverse phase fractionation was carried out on an Agilent 1200 Infinity high-performance liquid chromatography system, equipped with a Gemini C18 column (3 µm, 110 Å, 100 x 1.0 mm, Phenomenex).

Liquid Chromatography was performed on an UltiMate 3000 RSLC nano LC system (Dionex) fitted with a trapping cartridge (µ-Precolumn C18 PepMap 100, 5µm, 300 µm i.d. x 5 mm, 100 Å) and an analytical column (nanoEase™ M/Z HSS T3 column 75 µm x 250 mm C18, 1.8 µm, 100 Å, Waters). Trapping was carried out with a constant flow of 0.05% trifluoroacetic acid at 30 µL/min onto the trapping column for 6 minutes. Peptides were eluted from the analytical column through a constant flow of solvent A (0.1% formic acid in water) at 0.3 µL/min with increasing percentage of solvent B (0.1% formic acid in acetonitrile). The outlet of the analytical column was coupled directly to a Fusion Lumos (Thermo) mass spectrometer using the Nanospray Flex™ ion source in positive ion mode.

The peptides were introduced into the Fusion Lumos via a Pico-Tip Emitter 360 µm OD x 20 µm ID; 10 µm tip (New Objective) and an applied spray voltage of 2.4 kV. The capillary temperature was set at 275°C. Full mass scan (MS1) was acquired with mass range 375-1500 m/z in profile mode in the orbitrap with resolution of 60000. The filling time was set at maximum of 50 ms. Data dependent acquisition (DDA) was performed with the resolution of the Orbitrap set to 15000, with a fill time of 54 ms and a limitation of $1x10^5$ ions. A normalized collision energy of 36 was applied. MS^2 data was acquired in profile mode.

Data search (Isobarquant) and analysis

IsobarQuant[116] and Mascot (v2.2.07) were used to process the acquired data, which was searched against a Uniprot *Homo sapiens* proteome database (UP000005640) database containing common contaminants and reversed sequences. The following modifications were set into the search parameters: Carbamidomethyl (C) and TMT6 (K) (fixed modification), Acetyl (Protein N-term), Oxidation (M) and TMT6 (N-term) (variable modifications). For the full scan (MS1) a mass error tolerance of 10 ppm and for MS/MS (MS2) spectra of 0.02 Da was set. Further parameters were set: Trypsin as protease with an allowance of maximum two missed cleavages: a minimum peptide length of seven amino acids; at least two unique peptides were required for a protein to be identified. The false discovery rate on peptide and protein level was set to 0.01.

The raw output files of IsobarQuant were processed using the R programming language. Only proteins that were quantified with at least two unique peptides were considered for the analysis. Moreover, only proteins which were identified in two out of three mass spec runs were kept. 2415 proteins passed the quality control filters. Raw signal-sums (signal_sum columns) were first cleaned for batch effects using limma[106] and further normalized using vsn (variance stabilization normalization). Missing values were imputed with knn method using the Msnbase package. Proteins were tested for differential expression using the limma package. The replicate information was added as a factor in the design matrix given as an argument to the 'lmFit' function of limma. Also, imputed values were given a weight of 0.05 in the 'lmFit' function. A protein was annotated as a hit with a false discovery rate (fdr) smaller 5 % and a fold-change of at least 100 % and as a candidate with a fdr below 20 % and a fold-change of at least 50 %. PCA and Heatmap were generated with R software. Ontology analysis was performed with the Metascape tool (https://metascape.org/) applying standard parameters; non-relevant categories/pathways were omitted from the graphical representation.

Correlative Widefield - Super resolution STORM Microscopy

CENP-B DBD-ETAA1 AAD- AID cell line was seeded onto 22x22 coverslips and treated for 24h with IAA (0.5 µM), IAA and XL413 (10 µM), DOX (100 ng/mL), DOX and ATRi VE-821 (10 µM). After a 30 min pulse with EdU 10 µM, cells were fixed and stained according to the EdU labelling protocol (see dedicated section) using ACA antibody to mark centromeres, and Azide-Alexa Fluor 647 (1 µg/mL) (Invitrogen, A10277) to reveal EdU incorporation.

Samples were mounted on cavity slides (Sigma-Aldrich, BR475505) in fresh Abbelight buffer (Abbelight) and sealed with eco-sil speed (Rotec) to prevent oxygen entry. Imaging was done with an Abbelight SAFe360 and Neo_Acquisition software (Abbelight) mounted onto a Ti-E2 microscope with a 100X 1.49 NA TIRF objective (Nikon) and an ORCA-Fusion BT sCMOS camera (Hamamatsu), giving a final pixel size of 97 nm. Acquisitions were made in HiLO illumination mode. First, a Z-stack of the 488 nm green channel (centromeres) was acquired in widefield, with 200 nm step size, 21 steps, 150 ms exposure time. The focus was made onto an area with several bright centromeres on the same plane. A snapshot was taken for the centromeres, followed by one for the EdU signal in far red and a last for the DAPI (405 nm laser) for later nucleus segmentation. Then, the super resolution acquisition was made by increasing slowly the 640 nm laser power (540 mW, 3-4 kW/cm²) to 100% and wait for 10000 frames at 11 ms exposure time to start the acquisition (pumping phase). 60000 frames were acquired at 11 ms exposure time, to limit the overlap of blinking events due to the high density of EdU labelling. Each region of interest (ROI) was about 25 x 25 µm, with a laser scanning scale of 25 to focus the power on our ROI (Arbitrary unit from the Abbelight microscope settings, going from 0, no scan, to 100, the largest scanning region, covering roughly 150 x 150 µm²). Four to six nuclei were acquired per condition and three independent batches were assessed.

The movies were processed using Neo_Abbelight software (v38). The first 10000 frames were removed, and the 50000 remaining frames were kept for later processing. The data were filtered as followed: 20 nm maximum for uncertainty and a minimum of 500 nm for neighboring blinking distance to avoid overlap between two blinking events. The drift correction was made using the cross-correlation function with 1500 frames (stack size) and 25 nm as lateral pixel size. The merge of successive time ON was made using the following parameters: Least square fitting method (LSQ), 40 maximum consecutive frames and 1 maximum inactive frame. To clean the data from background localizations, a DBSCAN clustering was applied with a radius of 50 nm and a minimum of 10 localizations.

The area but not the intensity of incorporated EdU was used as proxy of the amount of incorporated EdU. Indeed, EdU labelling gives rise to extremely dense blinking events in the brightest areas. This results in a lot of blinking events that were discarded based on the minimum distance from two neighbors (500 nm). In addition, localization density presented variable parameters such as the pumping phase and the degree of labelling. Thus, the density of localization was not used as proxy of the amount of incorporated EdU.

Super resolution data analysis

An in-house MATLAB script was developed to analyze the data. First, the centromeres were segmented in 3D using the Z-stack to identify the centromeres in the focal plane from the corresponding snapshot. The nucleus was segmented using the DAPI channel. Then, the super resolution data were registered onto the widefield images using the EdU widefield snapshot with a correlation method. The area of the EdU localizations was evaluated using the alphaShape algorithm[117] with the smallest alpha radius to encompass all the detections. This unbiased method returns the point-cloud contours with high fidelity. The ratio of EdU area present in the segmented centromeres over the total area of the centromeres was calculated for each nucleus. The total EdU area outside the centromeres was evaluated and to the size of the nucleus (without the centromere areas). This way, we obtain the EdU signal specific to the centromeres and the general EdU signal in nucleus outside the centromeres.

The statistical analysis was done using a linear mixed model fit by REML on Jamovi software (https://www.jamovi.org. R Core Team (2021). The calculated ratios (centromeres or nucleus minus centromeres) are the dependent variables and treatment the independent variable (factors). The batch variable was considered as cluster variable and its intercept as random coefficient. The Holm post hoc test was used to compare the four conditions to each other.

Quantification and statistical analysis

Statistical analysis of all the graphs was performed using GraphPad Prism 9. A two-sided χ^2 test was performed on categorical datasets. t tests and Mann–Whitney U tests were respectively performed on quantitative datasets depending on whether they followed a normal distribution or not.

SUPPLEMENTARY TABLES

Supplementary Table 1. TMT-PICh output. Related to figure 4. The table is made by Limma package proteomics data analysis, as indicated in the Methods section. Log FC, false discover rate and p-value are indicated for each identified protein in the relative pairwise comparison.

Supplementary Table 2. Heatmaps of copy number segments from TCGA. Related to Figure 6. Heatmaps of copy number segments that cover more than 75% of the chromosome arm or that are covering part of both arms of a chromosome across the whole genome for the three cancer types. The colors represent the copy number categories of each segment.

Supplementary Table 3. Summary of the data presented in all the graphs. **Related to Figures 1 – 7.**

Supplementary Table 4. TCGA cancer type abbreviations and other types of abbreviations. **Related to Figure 6.** Table was adapted from https://gdc.cancer.gov/resources-tcga-users/tcga-code-tables/tcga-study-abbreviations.

REFERENCES

1. Taylor, A.M., Shih, J., Ha, G., Gao, G.F., Zhang, X., Berger, A.C., Schumacher, S.E., Wang, C., Hu, H., Liu, J., et al. (2018). Genomic and Functional Approaches to Understanding Cancer Aneuploidy. Cancer Cell *33*, 676-689 e673. 10.1016/j.ccell.2018.03.007.
2. Beroukhim, R., Mermel, C.H., Porter, D., Wei, G., Raychaudhuri, S., Donovan, J., Barretina, J., Boehm, J.S., Dobson, J., Urashima, M., et al. (2010). The landscape of somatic copy-number alteration across human cancers. Nature *463*, 899-905. 10.1038/nature08822.

3. Shih, J., Sarmashghi, S., Zhakula-Kostadinova, N., Zhang, S., Georgis, Y., Hoyt, S.H., Cuoco, M.S., Gao, G.F., Spurr, L.F., Berger, A.C., et al. (2023). Cancer aneuploidies are shaped primarily by effects on tumour fitness. Nature *619*, 793-800. 10.1038/s41586-023-06266-3.
4. Shukla, A., Nguyen, T.H.M., Moka, S.B., Ellis, J.J., Grady, J.P., Oey, H., Cristino, A.S., Khanna, K.K., Kroese, D.P., Krause, L., et al. (2020). Chromosome arm aneuploidies shape tumour evolution and drug response. Nat Commun *11*, 449. 10.1038/s41467-020-14286-0.
5. Altemose, N., Logsdon, G.A., Bzikadze, A.V., Sidhwani, P., Langley, S.A., Caldas, G.V., Hoyt, S.J., Uralsky, L., Ryabov, F.D., Shew, C.J., et al. (2022). Complete genomic and epigenetic maps of human centromeres. Science *376*, eabl4178. 10.1126/science.abl4178.
6. Gershman, A., Sauria, M.E.G., Guitart, X., Vollger, M.R., Hook, P.W., Hoyt, S.J., Jain, M., Shumate, A., Razaghi, R., Koren, S., et al. (2022). Epigenetic patterns in a complete human genome. Science *376*, eabj5089. 10.1126/science.abj5089.
7. Mellone, B.G., and Fachinetti, D. (2021). Diverse mechanisms of centromere specification. Curr Biol *31*, R1491-R1504. 10.1016/j.cub.2021.09.083.
8. Martinez, A.C., and van Wely, K.H. (2011). Centromere fission, not telomere erosion, triggers chromosomal instability in human carcinomas. Carcinogenesis *32*, 796-803. 10.1093/carcin/bgr069.
9. Barra, V., and Fachinetti, D. (2018). The dark side of centromeres: types, causes and consequences of structural abnormalities implicating centromeric DNA. Nat Commun *9*, 4340. 10.1038/s41467-018-06545-y.
10. Yilmaz, D., Furst, A., Meaburn, K., Lezaja, A., Wen, Y., Altmeyer, M., Reina-San-Martin, B., and Soutoglou, E. (2021). Activation of homologous recombination in G1 preserves centromeric integrity. Nature *600*, 748-753. 10.1038/s41586-021-04200-z.
11. Giunta, S., Herve, S., White, R.R., Wilhelm, T., Dumont, M., Scelfo, A., Gamba, R., Wong, C.K., Rancati, G., Smogorzewska, A., et al. (2021). CENP-A chromatin prevents replication stress at centromeres to avoid structural aneuploidy. Proc Natl Acad Sci U S A *118*. 10.1073/pnas.2015634118.
12. Crosetto, N., Mitra, A., Silva, M.J., Bienko, M., Dojer, N., Wang, Q., Karaca, E., Chiarle, R., Skrzypczak, M., Ginalski, K., et al. (2013). Nucleotide-resolution DNA double-strand break mapping by next-generation sequencing. Nat Methods *10*, 361-365. 10.1038/nmeth.2408.
13. Saayman, X., Graham, E., Nathan, W.J., Nussenzweig, A., and Esashi, F. (2023). Centromeres as universal hotspots of DNA breakage, driving RAD51-mediated recombination during quiescence. Mol Cell *83*, 523-538 e527. 10.1016/j.molcel.2023.01.004.
14. O'Keefe, R.T., Henderson, S.C., and Spector, D.L. (1992). Dynamic organization of DNA replication in mammalian cell nuclei: spatially and temporally defined replication of chromosome-specific alpha-satellite DNA sequences. J Cell Biol *116*, 1095-1110. 10.1083/jcb.116.5.1095.
15. Erliandri, I., Fu, H., Nakano, M., Kim, J.H., Miga, K.H., Liskovykh, M., Earnshaw, W.C., Masumoto, H., Kouprina, N., Aladjem, M.I., and Larionov, V. (2014). Replication of alpha-satellite DNA arrays in endogenous human centromeric regions and in human artificial chromosome. Nucleic Acids Res *42*, 11502-11516. 10.1093/nar/gku835.
16. Massey, D.J., and Koren, A. (2022). Telomere-to-telomere human DNA replication timing profiles. Sci Rep *12*, 9560. 10.1038/s41598-022-13638-8.
17. Kasinathan, S., and Henikoff, S. (2018). Non-B-Form DNA Is Enriched at Centromeres. Mol Biol Evol *35*, 949-962. 10.1093/molbev/msy010.
18. Balzano, E., Pelliccia, F., and Giunta, S. (2021). Genome (in)stability at tandem repeats. Semin Cell Dev Biol *113*, 97-112. 10.1016/j.semcdb.2020.10.003.
19. Mishra, P.K., Chakraborty, A., Yeh, E., Feng, W., Bloom, K.S., and Basrai, M.A. (2021). R-loops at centromeric chromatin contribute to defects in kinetochore integrity and chromosomal instability in budding yeast. Mol Biol Cell *32*, 74-89. 10.1091/mbc.E20-06-0379.
20. Kabeche, L., Nguyen, H.D., Buisson, R., and Zou, L. (2018). A mitosis-specific and R loop-driven ATR pathway promotes faithful chromosome segregation. Science *359*, 108-114. 10.1126/science.aan6490.
21. Wilhelm, T., Said, M., and Naim, V. (2020). DNA Replication Stress and Chromosomal Instability: Dangerous Liaisons. Genes (Basel) *11*. 10.3390/genes11060642.
22. Sackton, K.L., Dimova, N., Zeng, X., Tian, W., Zhang, M., Sackton, T.B., Meaders, J., Pfaff, K.L., Sigoillot, F., Yu, H., et al. (2014). Synergistic blockade of mitotic exit by two chemical inhibitors of the APC/C. Nature *514*, 646-649. 10.1038/nature13660.

23. Naim, V., Wilhelm, T., Debatisse, M., and Rosselli, F. (2013). ERCC1 and MUS81-EME1 promote sister chromatid separation by processing late replication intermediates at common fragile sites during mitosis. Nat Cell Biol *15*, 1008-1015. 10.1038/ncb2793.
24. Ying, S., Minocherhomji, S., Chan, K.L., Palmai-Pallag, T., Chu, W.K., Wass, T., Mankouri, H.W., Liu, Y., and Hickson, I.D. (2013). MUS81 promotes common fragile site expression. Nat Cell Biol *15*, 1001-1007. 10.1038/ncb2773.
25. Bianco, J.N., Bergoglio, V., Lin, Y.L., Pillaire, M.J., Schmitz, A.L., Gilhodes, J., Lusque, A., Mazieres, J., Lacroix-Triki, M., Roumeliotis, T.I., et al. (2019). Overexpression of Claspin and Timeless protects cancer cells from replication stress in a checkpoint-independent manner. Nat Commun *10*, 910. 10.1038/s41467-019-08886-8.
26. Jones, M.J.K., Rai, S.K., Pfuderer, P.L., Bonfim-Melo, A., Pagan, J.K., Clarke, P.R., McClelland, S.E., and Boemo, M.A. (2022). A high-resolution, nanopore-based artificial intelligence assay for DNA replication stress in human cancer cells. bioRxiv, 2022.2009.2022.509021. 10.1101/2022.09.22.509021.
27. Cheng, C.H., and Kuchta, R.D. (1993). DNA polymerase epsilon: aphidicolin inhibition and the relationship between polymerase and exonuclease activity. Biochemistry *32*, 8568-8574. 10.1021/bi00084a025.
28. Ikegami, S., Taguchi, T., Ohashi, M., Oguro, M., Nagano, H., and Mano, Y. (1978). Aphidicolin prevents mitotic cell division by interfering with the activity of DNA polymerase-alpha. Nature *275*, 458-460. 10.1038/275458a0.
29. Montagnoli, A., Valsasina, B., Croci, V., Menichincheri, M., Rainoldi, S., Marchesi, V., Tibolla, M., Tenca, P., Brotherton, D., Albanese, C., et al. (2008). A Cdc7 kinase inhibitor restricts initiation of DNA replication and has antitumor activity. Nat Chem Biol *4*, 357-365. 10.1038/nchembio.90.
30. Wassing, I.E., Graham, E., Saayman, X., Rampazzo, L., Ralf, C., Bassett, A., and Esashi, F. (2021). The RAD51 recombinase protects mitotic chromatin in human cells. Nat Commun *12*, 5380. 10.1038/s41467-021-25643-y.
31. Garribba, L., De Feudis, G., Martis, V., Galli, M., Dumont, M., Eliezer, Y., Wardenaar, R., Ippolito, M.R., Iyer, D.R., Tijhuis, A.E., et al. (2023). Short-term molecular consequences of chromosome mis-segregation for genome stability. Nat Commun *14*, 1353. 10.1038/s41467-023-37095-7.
32. Zhang, H., and Freudenreich, C.H. (2007). An AT-rich sequence in human common fragile site FRA16D causes fork stalling and chromosome breakage in S. cerevisiae. Mol Cell *27*, 367-379. 10.1016/j.molcel.2007.06.012.
33. Shah, S.N., Opresko, P.L., Meng, X., Lee, M.Y., and Eckert, K.A. (2010). DNA structure and the Werner protein modulate human DNA polymerase delta-dependent replication dynamics within the common fragile site FRA16D. Nucleic Acids Res *38*, 1149-1162. 10.1093/nar/gkp1131.
34. Bloom, K., and Costanzo, V. (2017). Centromere Structure and Function. Prog Mol Subcell Biol *56*, 515-539. 10.1007/978-3-319-58592-5_21.
35. Gallego, J., Chou, S.H., and Reid, B.R. (1997). Centromeric pyrimidine strands fold into an intercalated motif by forming a double hairpin with a novel T:G:G:T tetrad: solution structure of the d(TCCCGTTTCCA) dimer. J Mol Biol *273*, 840-856. 10.1006/jmbi.1997.1361.
36. Chardon, F., Japaridze, A., Witt, H., Velikovsky, L., Chakraborty, C., Wilhelm, T., Dumont, M., Yang, W., Kikuti, C., Gangnard, S., et al. (2022). CENP-B-mediated DNA loops regulate activity and stability of human centromeres. Mol Cell *82*, 1751-1767 e1758. 10.1016/j.molcel.2022.02.032.
37. Jonstrup, A.T., Thomsen, T., Wang, Y., Knudsen, B.R., Koch, J., and Andersen, A.H. (2008). Hairpin structures formed by alpha satellite DNA of human centromeres are cleaved by human topoisomerase IIalpha. Nucleic Acids Res *36*, 6165-6174. 10.1093/nar/gkn640.
38. Sugimura, K., Takebayashi, S., Taguchi, H., Takeda, S., and Okumura, K. (2008). PARP-1 ensures regulation of replication fork progression by homologous recombination on damaged DNA. J Cell Biol *183*, 1203-1212. 10.1083/jcb.200806068.
39. Maya-Mendoza, A., Moudry, P., Merchut-Maya, J.M., Lee, M., Strauss, R., and Bartek, J. (2018). High speed of fork progression induces DNA replication stress and genomic instability. Nature *559*, 279-284. 10.1038/s41586-018-0261-5.
40. Raso, M.C., Djoric, N., Walser, F., Hess, S., Schmid, F.M., Burger, S., Knobeloch, K.P., and Penengo, L. (2020). Interferon-stimulated gene 15 accelerates replication fork progression inducing chromosomal breakage. J Cell Biol *219*. 10.1083/jcb.202002175.
41. Berti, M., Ray Chaudhuri, A., Thangavel, S., Gomathinayagam, S., Kenig, S., Vujanovic, M., Odreman, F., Glatter, T., Graziano, S., Mendoza-Maldonado, R., et al. (2013). Human RECQ1 promotes restart of

replication forks reversed by DNA topoisomerase I inhibition. Nat Struct Mol Biol *20*, 347-354. 10.1038/nsmb.2501.

42. Murillo-Pineda, M., Valente, L.P., Dumont, M., Mata, J.F., Fachinetti, D., and Jansen, L.E.T. (2021). Induction of spontaneous human neocentromere formation and long-term maturation. J Cell Biol *220*. 10.1083/jcb.202007210.
43. Yoda, K., Kitagawa, K., Masumoto, H., Muro, Y., and Okazaki, T. (1992). A human centromere protein, CENP-B, has a DNA binding domain containing four potential alpha helices at the NH2 terminus, which is separable from dimerizing activity. J Cell Biol *119*, 1413-1427. 10.1083/jcb.119.6.1413.
44. Saldivar, J.C., Cortez, D., and Cimprich, K.A. (2017). The essential kinase ATR: ensuring faithful duplication of a challenging genome. Nat Rev Mol Cell Biol *18*, 622-636. 10.1038/nrm.2017.67.
45. Aze, A., Sannino, V., Soffientini, P., Bachi, A., and Costanzo, V. (2016). Centromeric DNA replication reconstitution reveals DNA loops and ATR checkpoint suppression. Nat Cell Biol *18*, 684-691. 10.1038/ncb3344.
46. Atashpaz, S., Samadi Shams, S., Gonzalez, J.M., Sebestyen, E., Arghavanifard, N., Gnocchi, A., Albers, E., Minardi, S., Faga, G., Soffientini, P., et al. (2020). ATR expands embryonic stem cell fate potential in response to replication stress. Elife *9*. 10.7554/eLife.54756.
47. Li, Y., Xue, B., Zhang, M., Zhang, L., Hou, Y., Qin, Y., Long, H., Su, Q.P., Wang, Y., Guan, X., et al. (2021). Transcription-coupled structural dynamics of topologically associating domains regulate replication origin efficiency. Genome Biol *22*, 206. 10.1186/s13059-021-02424-w.
48. Nishimura, K., Fukagawa, T., Takisawa, H., Kakimoto, T., and Kanemaki, M. (2009). An auxin-based degron system for the rapid depletion of proteins in nonplant cells. Nat Methods *6*, 917-922. 10.1038/nmeth.1401.
49. Ward, I.M., and Chen, J. (2001). Histone H2AX is phosphorylated in an ATR-dependent manner in response to replicational stress. J Biol Chem *276*, 47759-47762. 10.1074/jbc.C100569200.
50. Dewar, J.M., and Walter, J.C. (2017). Mechanisms of DNA replication termination. Nat Rev Mol Cell Biol *18*, 507-516. 10.1038/nrm.2017.42.
51. Dejardin, J., and Kingston, R.E. (2009). Purification of proteins associated with specific genomic Loci. Cell *136*, 175-186. 10.1016/j.cell.2008.11.045.
52. Saksouk, N., Barth, T.K., Ziegler-Birling, C., Olova, N., Nowak, A., Rey, E., Mateos-Langerak, J., Urbach, S., Reik, W., Torres-Padilla, M.E., et al. (2014). Redundant mechanisms to form silent chromatin at pericentromeric regions rely on BEND3 and DNA methylation. Mol Cell *56*, 580-594. 10.1016/j.molcel.2014.10.001.
53. Hoffmann, S., Dumont, M., Barra, V., Ly, P., Nechemia-Arbely, Y., McMahon, M.A., Herve, S., Cleveland, D.W., and Fachinetti, D. (2016). CENP-A Is Dispensable for Mitotic Centromere Function after Initial Centromere/Kinetochore Assembly. Cell Rep *17*, 2394-2404. 10.1016/j.celrep.2016.10.084.
54. McKinley, K.L., and Cheeseman, I.M. (2016). The molecular basis for centromere identity and function. Nat Rev Mol Cell Biol *17*, 16-29. 10.1038/nrm.2015.5.
55. Dumont, M., and Fachinetti, D. (2017). DNA Sequences in Centromere Formation and Function. Prog Mol Subcell Biol *56*, 305-336. 10.1007/978-3-319-58592-5_13.
56. Baxter, J., and Diffley, J.F. (2008). Topoisomerase II inactivation prevents the completion of DNA replication in budding yeast. Mol Cell *30*, 790-802. 10.1016/j.molcel.2008.04.019.
57. Deegan, T.D., Baxter, J., Ortiz Bazan, M.A., Yeeles, J.T.P., and Labib, K.P.M. (2019). Pif1-Family Helicases Support Fork Convergence during DNA Replication Termination in Eukaryotes. Mol Cell *74*, 231-244 e239. 10.1016/j.molcel.2019.01.040.
58. Fachinetti, D., Bermejo, R., Cocito, A., Minardi, S., Katou, Y., Kanoh, Y., Shirahige, K., Azvolinsky, A., Zakian, V.A., and Foiani, M. (2010). Replication termination at eukaryotic chromosomes is mediated by Top2 and occurs at genomic loci containing pausing elements. Mol Cell *39*, 595-605. 10.1016/j.molcel.2010.07.024.
59. Chan, Y.W., and West, S.C. (2018). A new class of ultrafine anaphase bridges generated by homologous recombination. Cell Cycle *17*, 2101-2109. 10.1080/15384101.2018.1515555.
60. Broderick, R., Nieminuszczy, J., Blackford, A.N., Winczura, A., and Niedzwiedz, W. (2015). TOPBP1 recruits TOP2A to ultra-fine anaphase bridges to aid in their resolution. Nat Commun *6*, 6572. 10.1038/ncomms7572.
61. Bagge, J., Oestergaard, V.H., and Lisby, M. (2021). Functions of TopBP1 in preserving genome integrity during mitosis. Semin Cell Dev Biol *113*, 57-64. 10.1016/j.semcdb.2020.08.009.

62. Fekairi, S., Scaglione, S., Chahwan, C., Taylor, E.R., Tissier, A., Coulon, S., Dong, M.Q., Ruse, C., Yates, J.R., 3rd, Russell, P., et al. (2009). Human SLX4 is a Holliday junction resolvase subunit that binds multiple DNA repair/recombination endonucleases. Cell *138*, 78-89. 10.1016/j.cell.2009.06.029.
63. Munoz, I.M., Hain, K., Declais, A.C., Gardiner, M., Toh, G.W., Sanchez-Pulido, L., Heuckmann, J.M., Toth, R., Macartney, T., Eppink, B., et al. (2009). Coordination of structure-specific nucleases by human SLX4/BTBD12 is required for DNA repair. Mol Cell *35*, 116-127. 10.1016/j.molcel.2009.06.020.
64. Kolas, N.K., Svetlanov, A., Lenzi, M.L., Macaluso, F.P., Lipkin, S.M., Liskay, R.M., Greally, J., Edelmann, W., and Cohen, P.E. (2005). Localization of MMR proteins on meiotic chromosomes in mice indicates distinct functions during prophase I. J Cell Biol *171*, 447-458. 10.1083/jcb.200506170.
65. Young, S.J., Sebald, M., Shah Punatar, R., Larin, M., Masino, L., Rodrigo-Brenni, M.C., Liang, C.C., and West, S.C. (2020). MutSbeta Stimulates Holliday Junction Resolution by the SMX Complex. Cell Rep *33*, 108289. 10.1016/j.celrep.2020.108289.
66. Raschle, M., Smeenk, G., Hansen, R.K., Temu, T., Oka, Y., Hein, M.Y., Nagaraj, N., Long, D.T., Walter, J.C., Hofmann, K., et al. (2015). DNA repair. Proteomics reveals dynamic assembly of repair complexes during bypass of DNA cross-links. Science *348*, 1253671. 10.1126/science.1253671.
67. Hedglin, M., and Benkovic, S.J. (2015). Regulation of Rad6/Rad18 Activity During DNA Damage Tolerance. Annu Rev Biophys *44*, 207-228. 10.1146/annurev-biophys-060414-033841.
68. Bienko, M., Green, C.M., Crosetto, N., Rudolf, F., Zapart, G., Coull, B., Kannouche, P., Wider, G., Peter, M., Lehmann, A.R., et al. (2005). Ubiquitin-binding domains in Y-family polymerases regulate translesion synthesis. Science *310*, 1821-1824. 10.1126/science.1120615.
69. Venegas, A.B., Natsume, T., Kanemaki, M., and Hickson, I.D. (2020). Inducible Degradation of the Human SMC5/6 Complex Reveals an Essential Role Only during Interphase. Cell Rep *31*, 107533. 10.1016/j.celrep.2020.107533.
70. Wu, K.Z., Wang, G.N., Fitzgerald, J., Quachthithu, H., Rainey, M.D., Cattaneo, A., Bachi, A., and Santocanale, C. (2016). DDK dependent regulation of TOP2A at centromeres revealed by a chemical genetics approach. Nucleic Acids Res *44*, 8786-8798. 10.1093/nar/gkw626.
71. Nielsen, C.F., Zhang, T., Barisic, M., Kalitsis, P., and Hudson, D.F. (2020). Topoisomerase IIalpha is essential for maintenance of mitotic chromosome structure. Proc Natl Acad Sci U S A *117*, 12131-12142. 10.1073/pnas.2001760117.
72. Menolfi, D., Delamarre, A., Lengronne, A., Pasero, P., and Branzei, D. (2015). Essential Roles of the Smc5/6 Complex in Replication through Natural Pausing Sites and Endogenous DNA Damage Tolerance. Mol Cell *60*, 835-846. 10.1016/j.molcel.2015.10.023.
73. Yesbolatova, A., Saito, Y., Kitamoto, N., Makino-Itou, H., Ajima, R., Nakano, R., Nakaoka, H., Fukui, K., Gamo, K., Tominari, Y., et al. (2020). The auxin-inducible degron 2 technology provides sharp degradation control in yeast, mammalian cells, and mice. Nat Commun *11*, 5701. 10.1038/s41467-020-19532-z.
74. Kanda, R., Eguchi-Kasai, K., and Hayata, I. (1999). Phosphatase inhibitors and premature chromosome condensation in human peripheral lymphocytes at different cell-cycle phases. Somat Cell Mol Genet *25*, 1-8. 10.1023/b:scam.0000007135.12486.e3.
75. Yang, W., and Gao, Y. (2018). Translesion and Repair DNA Polymerases: Diverse Structure and Mechanism. Annu Rev Biochem *87*, 239-261. 10.1146/annurev-biochem-062917-012405.
76. Ben Yamin, B., Ahmed-Seghir, S., Tomida, J., Despras, E., Pouvelle, C., Yurchenko, A., Goulas, J., Corre, R., Delacour, Q., Droin, N., et al. (2021). DNA polymerase zeta contributes to heterochromatin replication to prevent genome instability. EMBO J *40*, e104543. 10.15252/embj.2020104543.
77. Wojtaszek, J.L., Chatterjee, N., Najeeb, J., Ramos, A., Lee, M., Bian, K., Xue, J.Y., Fenton, B.A., Park, H., Li, D., et al. (2019). A Small Molecule Targeting Mutagenic Translesion Synthesis Improves Chemotherapy. Cell *178*, 152-159 e111. 10.1016/j.cell.2019.05.028.
78. Steele, C.D., Abbasi, A., Islam, S.M.A., Bowes, A.L., Khandekar, A., Haase, K., Hames-Fathi, S., Ajayi, D., Verfaillie, A., Dhami, P., et al. (2022). Signatures of copy number alterations in human cancer. Nature *606*, 984-991. 10.1038/s41586-022-04738-6.
79. Barnes, B.M., Nelson, L., Tighe, A., Burghel, G.J., Lin, I.H., Desai, S., McGrail, J.C., Morgan, R.D., and Taylor, S.S. (2021). Distinct transcriptional programs stratify ovarian cancer cell lines into the five major histological subtypes. Genome Med *13*, 140. 10.1186/s13073-021-00952-5.
80. Coulson-Gilmer, C., Morgan, R.D., Nelson, L., Barnes, B.M., Tighe, A., Wardenaar, R., Spierings, D.C.J., Schlecht, H., Burghel, G.J., Foijer, F., et al. (2021). Replication catastrophe is responsible for intrinsic PAR glycohydrolase inhibitor-sensitivity in patient-derived ovarian cancer models. J Exp Clin Cancer Res *40*, 323. 10.1186/s13046-021-02124-0.

81. Nelson, L., Tighe, A., Golder, A., Littler, S., Bakker, B., Moralli, D., Murtuza Baker, S., Donaldson, I.J., Spierings, D.C.J., Wardenaar, R., et al. (2020). A living biobank of ovarian cancer ex vivo models reveals profound mitotic heterogeneity. Nat Commun *11*, 822. 10.1038/s41467-020-14551-2.
82. Cheasley, D., Nigam, A., Zethoven, M., Hunter, S., Etemadmoghadam, D., Semple, T., Allan, P., Carey, M.S., Fernandez, M.L., Dawson, A., et al. (2021). Genomic analysis of low-grade serous ovarian carcinoma to identify key drivers and therapeutic vulnerabilities. J Pathol *253*, 41-54. 10.1002/path.5545.
83. Brown, J., and Frumovitz, M. (2014). Mucinous tumors of the ovary: current thoughts on diagnosis and management. Curr Oncol Rep *16*, 389. 10.1007/s11912-014-0389-x.
84. Shih, I.M., Wang, Y., and Wang, T.L. (2021). The Origin of Ovarian Cancer Species and Precancerous Landscape. Am J Pathol *191*, 26-39. 10.1016/j.ajpath.2020.09.006.
85. Guerrero Llobet, S., Bhattacharya, A., Everts, M., Kok, K., van der Vegt, B., Fehrmann, R.S.N., and van Vugt, M. (2022). An mRNA expression-based signature for oncogene-induced replication-stress. Oncogene *41*, 1216-1224. 10.1038/s41388-021-02162-0.
86. Bakker, B., Taudt, A., Belderbos, M.E., Porubsky, D., Spierings, D.C., de Jong, T.V., Halsema, N., Kazemier, H.G., Hoekstra-Wakker, K., Bradley, A., et al. (2016). Single-cell sequencing reveals karyotype heterogeneity in murine and human malignancies. Genome Biol *17*, 115. 10.1186/s13059-016-0971-7.
87. Greenman, C.D., Cooke, S.L., Marshall, J., Stratton, M.R., and Campbell, P.J. (2016). Modeling the evolution space of breakage fusion bridge cycles with a stochastic folding process. J Math Biol *72*, 47-86. 10.1007/s00285-015-0875-2.
88. Giunta, S. (2018). Centromere Chromosome Orientation Fluorescent in situ Hybridization (Cen-CO-FISH) Detects Sister Chromatid Exchange at the Centromere in Human Cells. Bio Protoc *8*, e2792. 10.21769/BioProtoc.2792.
89. Negrini, S., Gorgoulis, V.G., and Halazonetis, T.D. (2010). Genomic instability--an evolving hallmark of cancer. Nat Rev Mol Cell Biol *11*, 220-228. 10.1038/nrm2858.
90. Scelfo, A., and Fachinetti, D. (2023). Centromere: A Trojan horse for genome stability. DNA Repair (Amst) *130*, 103569. 10.1016/j.dnarep.2023.103569.
91. Lawrimore, J., and Bloom, K. (2022). Shaping centromeres to resist mitotic spindle forces. J Cell Sci *135*. 10.1242/jcs.259532.
92. Keszthelyi, A., Minchell, N.E., and Baxter, J. (2016). The Causes and Consequences of Topological Stress during DNA Replication. Genes (Basel) *7*. 10.3390/genes7120134.
93. Zhong, Y., Nellimoottil, T., Peace, J.M., Knott, S.R., Villwock, S.K., Yee, J.M., Jancuska, J.M., Rege, S., Tecklenburg, M., Sclafani, R.A., et al. (2013). The level of origin firing inversely affects the rate of replication fork progression. J Cell Biol *201*, 373-383. 10.1083/jcb.201208060.
94. Ozer, O., and Hickson, I.D. (2018). Pathways for maintenance of telomeres and common fragile sites during DNA replication stress. Open Biol *8*. 10.1098/rsob.180018.
95. Ozeri-Galai, E., Lebofsky, R., Rahat, A., Bester, A.C., Bensimon, A., and Kerem, B. (2011). Failure of origin activation in response to fork stalling leads to chromosomal instability at fragile sites. Mol Cell *43*, 122-131. 10.1016/j.molcel.2011.05.019.
96. Heintzman, D.R., Campos, L.V., Byl, J.A.W., Osheroff, N., and Dewar, J.M. (2019). Topoisomerase II Is Crucial for Fork Convergence during Vertebrate Replication Termination. Cell Rep *29*, 422-436 e425. 10.1016/j.celrep.2019.08.097.
97. Irmisch, A., Ampatzidou, E., Mizuno, K., O'Connell, M.J., and Murray, J.M. (2009). Smc5/6 maintains stalled replication forks in a recombination-competent conformation. EMBO J *28*, 144-155. 10.1038/emboj.2008.273.
98. Agashe, S., Joseph, C.R., Reyes, T.A.C., Menolfi, D., Giannattasio, M., Waizenegger, A., Szakal, B., and Branzei, D. (2021). Smc5/6 functions with Sgs1-Top3-Rmi1 to complete chromosome replication at natural pause sites. Nat Commun *12*, 2111. 10.1038/s41467-021-22217-w.
99. Bonnell, E., Pasquier, E., and Wellinger, R.J. (2021). Telomere Replication: Solving Multiple End Replication Problems. Front Cell Dev Biol *9*, 668171. 10.3389/fcell.2021.668171.
100. Forment, J.V., Blasius, M., Guerini, I., and Jackson, S.P. (2011). Structure-specific DNA endonuclease Mus81/Eme1 generates DNA damage caused by Chk1 inactivation. PLoS One *6*, e23517. 10.1371/journal.pone.0023517.
101. Seplyarskiy, V.B., Bazykin, G.A., and Soldatov, R.A. (2015). Polymerase zeta Activity Is Linked to Replication Timing in Humans: Evidence from Mutational Signatures. Mol Biol Evol *32*, 3158-3172. 10.1093/molbev/msv184.

102. Miga, K.H., and Alexandrov, I.A. (2021). Variation and Evolution of Human Centromeres: A Field Guide and Perspective. Annu Rev Genet *55*, 583-602. 10.1146/annurev-genet-071719-020519.
103. Ben-David, U., and Amon, A. (2020). Context is everything: aneuploidy in cancer. Nat Rev Genet *21*, 44-62. 10.1038/s41576-019-0171-x.
104. Dessau, R.B., and Pipper, C.B. (2008). ["R"--project for statistical computing]. Ugeskr Laeger *170*, 328-330.
105. Breitwieser, F.P., and Colinge, J. (2013). Isobar(PTM): a software tool for the quantitative analysis of post-translationally modified proteins. J Proteomics *90*, 77-84. 10.1016/j.jprot.2013.02.022.
106. Ritchie, M.E., Phipson, B., Wu, D., Hu, Y., Law, C.W., Shi, W., and Smyth, G.K. (2015). limma powers differential expression analyses for RNA-sequencing and microarray studies. Nucleic Acids Res *43*, e47. 10.1093/nar/gkv007.
107. Perez-Riverol, Y., Bai, J., Bandla, C., Garcia-Seisdedos, D., Hewapathirana, S., Kamatchinathan, S., Kundu, D.J., Prakash, A., Frericks-Zipper, A., Eisenacher, M., et al. (2022). The PRIDE database resources in 2022: a hub for mass spectrometry-based proteomics evidences. Nucleic Acids Res *50*, D543-D552. 10.1093/nar/gkab1038.
108. Fellmann, C., Hoffmann, T., Sridhar, V., Hopfgartner, B., Muhar, M., Roth, M., Lai, D.Y., Barbosa, I.A., Kwon, J.S., Guan, Y., et al. (2013). An optimized microRNA backbone for effective single-copy RNAi. Cell Rep *5*, 1704-1713. 10.1016/j.celrep.2013.11.020.
109. Trott, J., Tan, E.K., Ong, S., Titmarsh, D.M., Denil, S., Giam, M., Wong, C.K., Wang, J., Shboul, M., Eio, M., et al. (2017). Long-Term Culture of Self-renewing Pancreatic Progenitors Derived from Human Pluripotent Stem Cells. Stem Cell Reports *8*, 1675-1688. 10.1016/j.stemcr.2017.05.019.
110. Gallo, D., Wang, G., Yip, C.M., and Brown, G.W. (2016). Analysis of Replicating Yeast Chromosomes by DNA Combing. Cold Spring Harb Protoc *2016*, pdb prot085118. 10.1101/pdb.prot085118.
111. Kilgas, S., Kiltie, A.E., and Ramadan, K. (2021). Immunofluorescence microscopy-based detection of ssDNA foci by BrdU in mammalian cells. STAR Protoc *2*, 100978. 10.1016/j.xpro.2021.100978.
112. Kan, S.L., Saksouk, N., and Dejardin, J. (2017). Proteome Characterization of a Chromatin Locus Using the Proteomics of Isolated Chromatin Segments Approach. Methods Mol Biol *1550*, 19-33. 10.1007/978-1-4939-6747-6_3.
113. Hughes, C.S., Foehr, S., Garfield, D.A., Furlong, E.E., Steinmetz, L.M., and Krijgsveld, J. (2014). Ultrasensitive proteome analysis using paramagnetic bead technology. Mol Syst Biol *10*, 757. 10.15252/msb.20145625.
114. Hughes, C.S., Moggridge, S., Muller, T., Sorensen, P.H., Morin, G.B., and Krijgsveld, J. (2019). Single-pot, solid-phase-enhanced sample preparation for proteomics experiments. Nat Protoc *14*, 68-85. 10.1038/s41596-018-0082-x.
115. Dayon, L., Hainard, A., Licker, V., Turck, N., Kuhn, K., Hochstrasser, D.F., Burkhard, P.R., and Sanchez, J.C. (2008). Relative quantification of proteins in human cerebrospinal fluids by MS/MS using 6-plex isobaric tags. Anal Chem *80*, 2921-2931. 10.1021/ac702422x.
116. Franken, H., Mathieson, T., Childs, D., Sweetman, G.M., Werner, T., Togel, I., Doce, C., Gade, S., Bantscheff, M., Drewes, G., et al. (2015). Thermal proteome profiling for unbiased identification of direct and indirect drug targets using multiplexed quantitative mass spectrometry. Nat Protoc *10*, 1567-1593. 10.1038/nprot.2015.101.
117. Edelsbrunner, H., Kirkpatrick, D., and Seidel, R. (1983). On the shape of a set of points in the plane. IEEE Transactions on information theory *29*, 551-559.

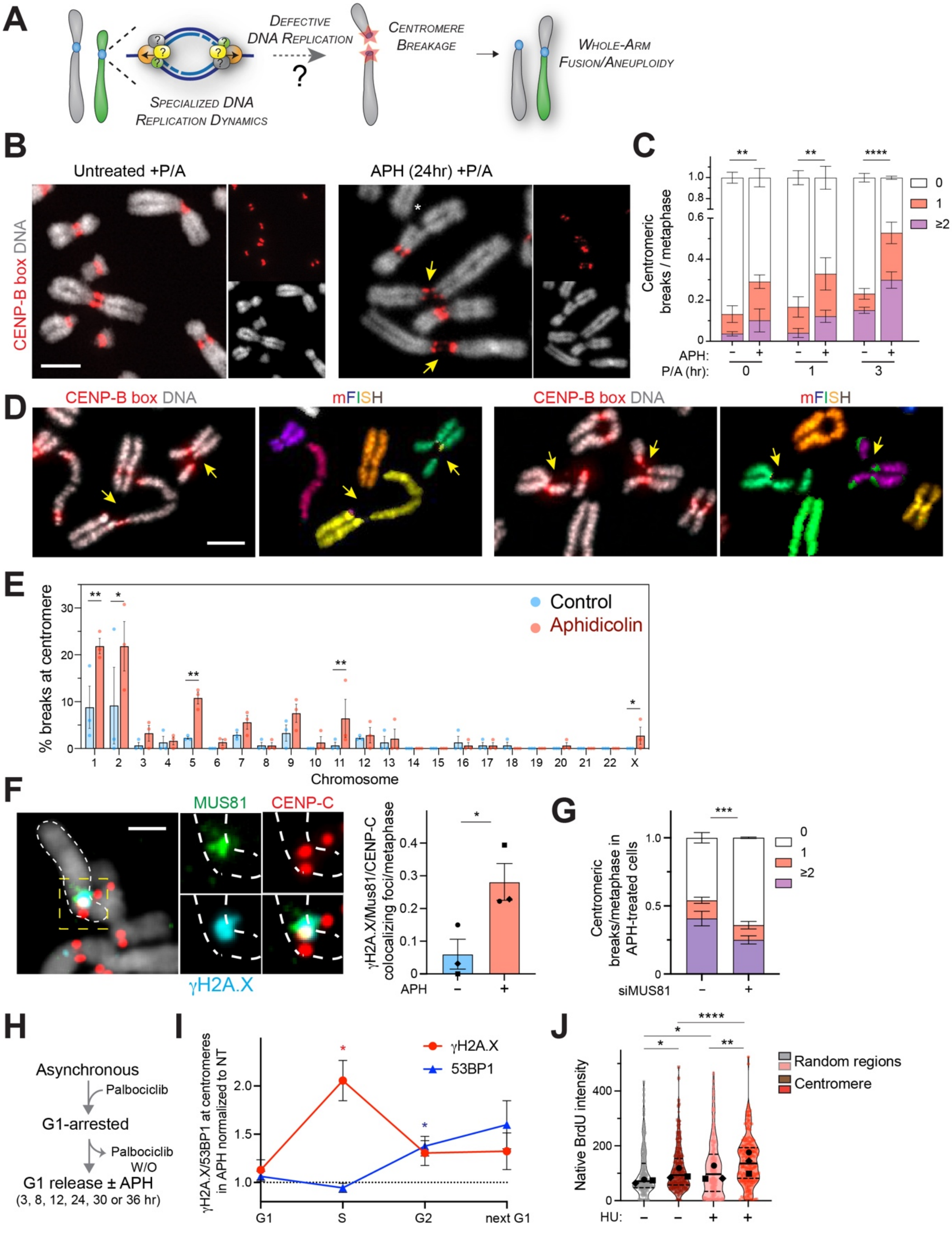
A
Specialized DNA Replication Dynamics
Defective DNA Replication
?
Centromere Breakage
Whole-Arm Fusion/Aneuploidy
B
Untreated +P/A
APH (24hr) +P/A
CENP-B box DNA
C
Centromeric breaks / metaphase
1.0
0.8
0.6
0.4
0.2
0
0
1
≥2
APH:
P/A (hr):
**
****
D
CENP-B box DNA
mFISH
E
% breaks at centromere
Control
Aphidicolin
Chromosome
1 2 3 4 5 6 7 8 9 10 11 12 13 14 15 16 17 18 19 20 21 22 X
F
MUS81
CENP-C
γH2A.X
γH2A.X/Mus81/CENP-C colocalizing foci/metaphase
APH
G
Centromeric breaks/metaphase in APH-treated cells
siMUS81
***
H
Asynchronous
Palbociclib
G1-arrested
Palbociclib W/O
G1 release ± APH
(3, 8, 12, 24, 30 or 36 hr)
I
γH2A.X/53BP1 at centromeres in APH normalized to NT
γH2A.X
53BP1
G1
S
G2
next G1
J
Native BrdU intensity
Random regions
Centromere
HU:

Figure 1

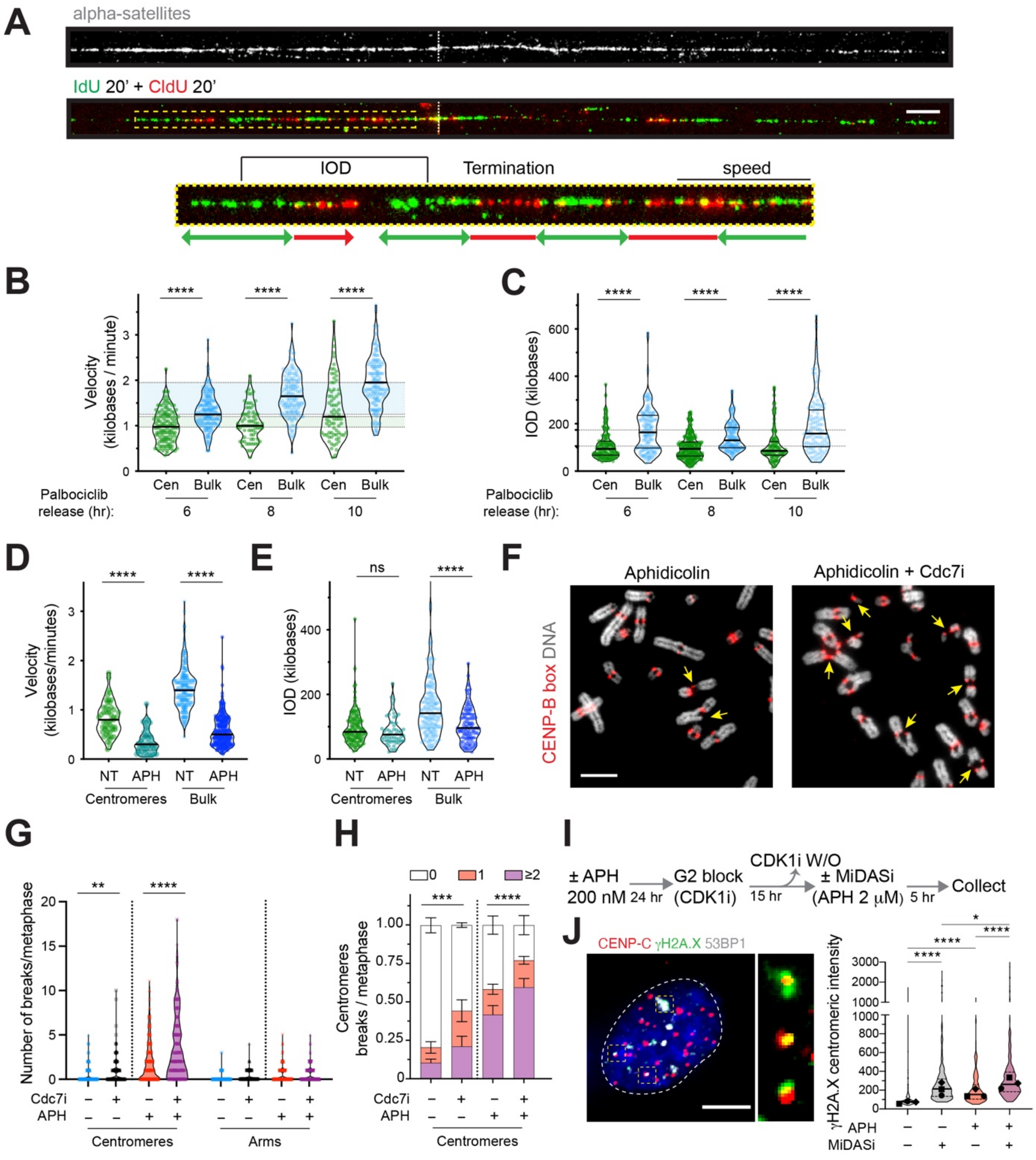
A
alpha-satellites
IdU 20' + CldU 20'
IOD
Termination
speed
B
Velocity (kilobases / minute)
0
1
2
3
****
****
****
Cen
Bulk
Cen
Bulk
Cen
Bulk
Palbociclib release (hr):
6
8
10
C
IOD (kilobases)
0
200
400
600
****
****
****
Cen
Bulk
Cen
Bulk
Cen
Bulk
Palbociclib release (hr):
6
8
10
D
Velocity (kilobases/minutes)
0
1
2
3
****
****
NT
APH
NT
APH
Centromeres
Bulk
E
IOD (kilobases)
0
200
400
ns
****
NT
APH
NT
APH
Centromeres
Bulk
F
Aphidicolin
Aphidicolin + Cdc7i
CENP-B box DNA
G
Number of breaks/metaphase
0
5
10
15
20
**
****
Cdc7i – + – + – + – +
APH – – + + – – + +
Centromeres
Arms
H
0
1
≥2
Centromeres breaks / metaphase
0
0.25
0.50
0.75
1.00
***
****
Cdc7i – + – +
APH – – + +
Centromeres
I
± APH 200 nM
24 hr
G2 block (CDK1i)
CDK1i W/O
15 hr
± MiDASi (APH 2 μM)
5 hr
Collect
J
CENP-C γH2A.X 53BP1
γH2A.X centromeric intensity
0
200
400
600
800
1000
1000
2000
3000
****
****
****
*
APH – – + +
MiDASi – + – +

Figure 2

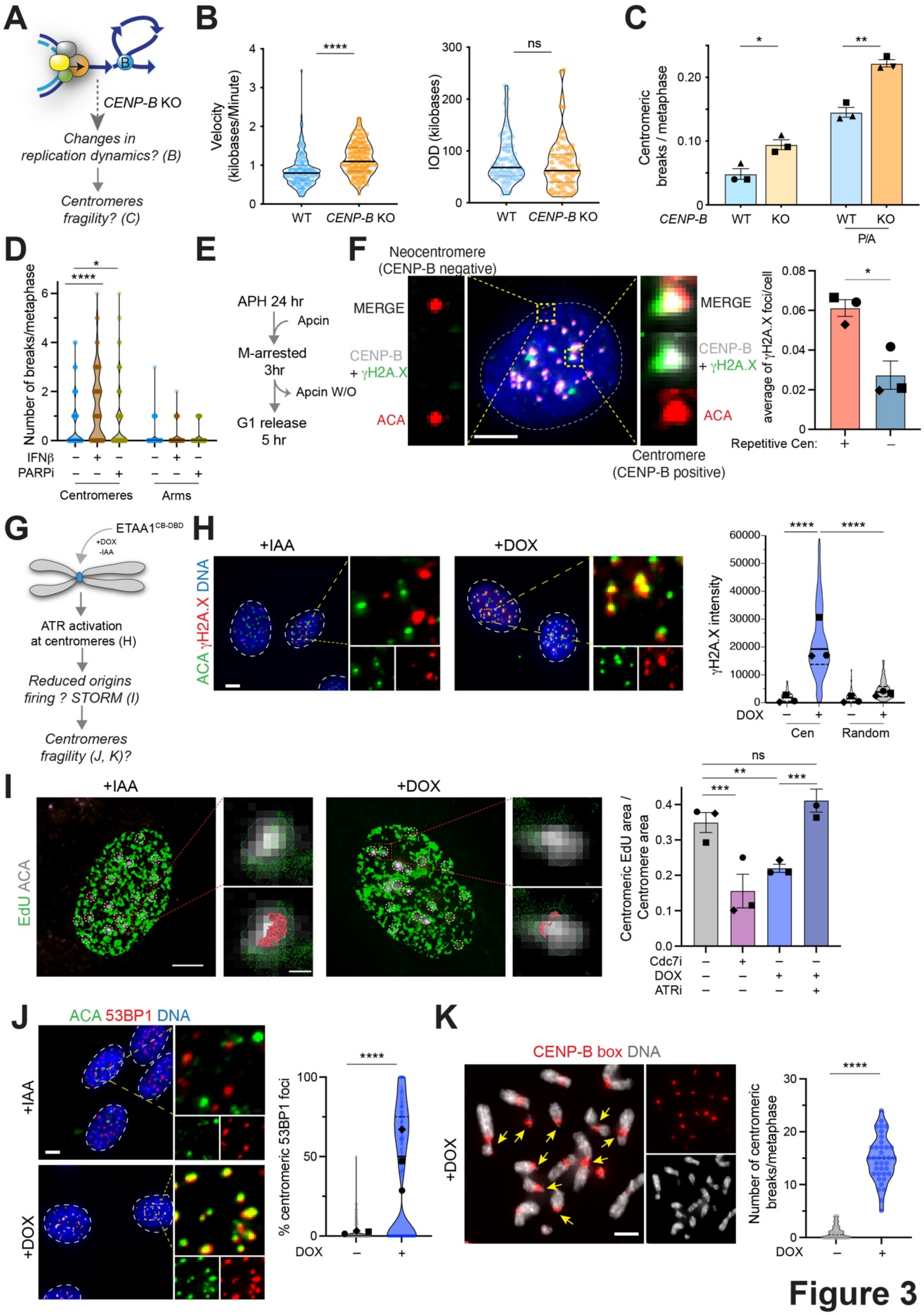
A
CENP-B KO
Changes in replication dynamics? (B)
Centromeres fragility? (C)
B
Velocity (kilobases/Minute)
IOD (kilobases)
****
ns
WT
CENP-B KO
C
Centromeric breaks / metaphase
*
**
CENP-B
WT
KO
P/A
D
Number of breaks/metaphase
IFNβ
PARPi
Centromeres
Arms
E
APH 24 hr
Apcin
M-arrested 3hr
Apcin W/O
G1 release 5 hr
F
Neocentromere (CENP-B negative)
MERGE
CENP-B + γH2A.X
ACA
Centromere (CENP-B positive)
average of γH2A.X foci/cell
Repetitive Cen:
G
ETAA1^{CB-DBD}
+DOX -IAA
ATR activation at centromeres (H)
Reduced origins firing ? STORM (I)
Centromeres fragility (J, K)?
H
+IAA
+DOX
ACA γH2A.X DNA
γH2A.X intensity
DOX
Cen
Random
I
EdU ACA
Centromeric EdU area / Centromere area
Cdc7i
DOX
ATRi
***
**
ns
J
ACA 53BP1 DNA
% centromeric 53BP1 foci
K
CENP-B box DNA
Number of centromeric breaks/metaphase

Figure 3

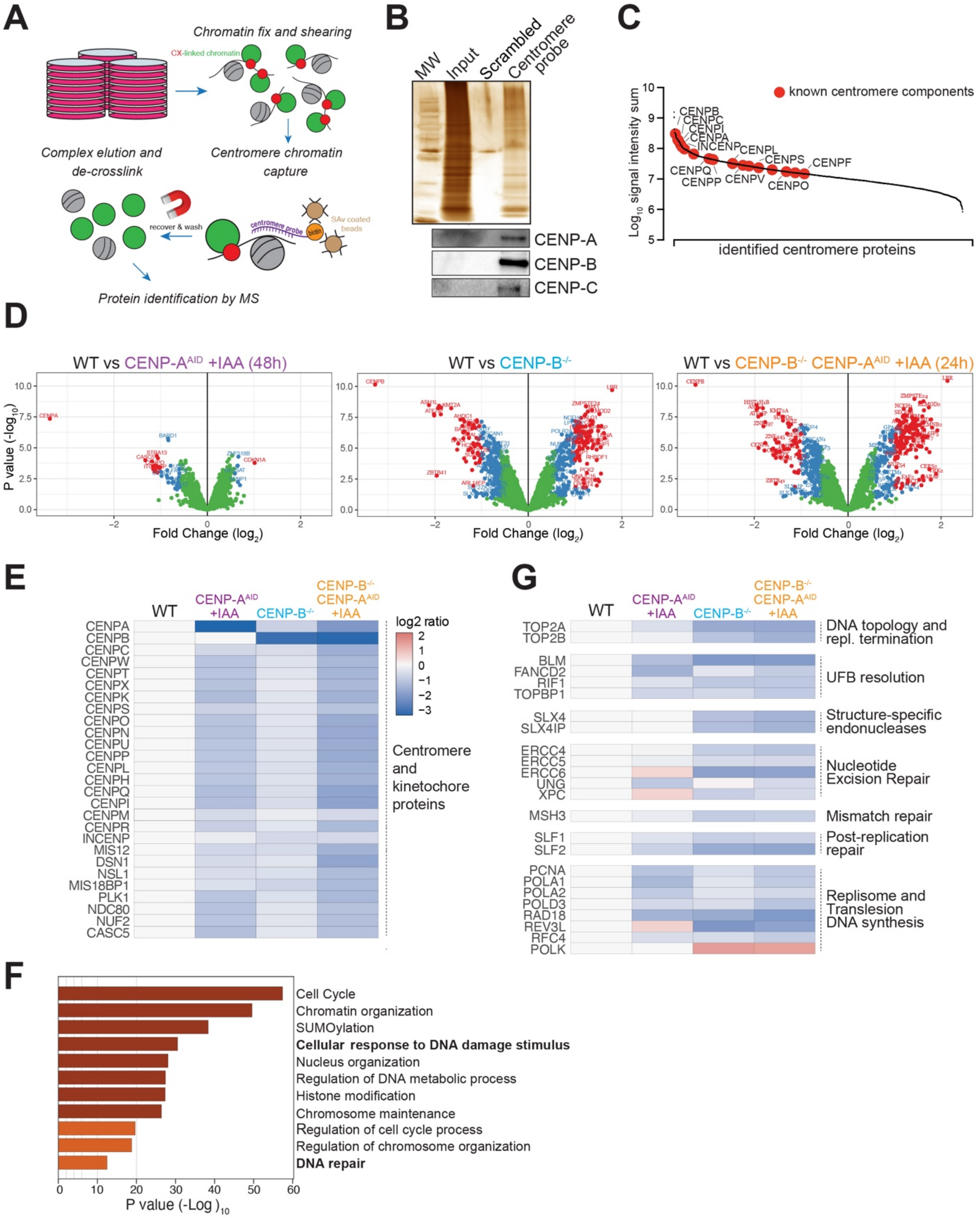
A
Chromatin fix and shearing
CX-linked chromatin
Centromere chromatin capture
Complex elution and de-crosslink
recover & wash
centromere probe
biotin
SAv coated beads
Protein identification by MS
B
MW
Input
Scrambled
Centromere probe
CENP-A
CENP-B
CENP-C
C
known centromere components
Log10 signal intensity sum
10
9
8
7
6
5
CENPB
CENPC
CENPI
CENPA
INCENP
CENPL
CENPS
CENPF
CENPQ
CENPP
CENPV
CENPO
identified centromere proteins
D
WT vs CENP-A^AID +IAA (48h)
WT vs CENP-B-/-
WT vs CENP-B-/- CENP-A^AID +IAA (24h)
P value (-log10)
Fold Change (log2)
10.0
7.5
5.0
2.5
0.0
-2
0
2
CENPA
CENPB
LBR
E
WT
CENP-A^AID +IAA
CENP-B-/-
CENP-B-/- CENP-A^AID +IAA
log2 ratio
2
1
0
−1
−2
−3
CENPA
CENPB
CENPC
CENPW
CENPT
CENPX
CENPK
CENPS
CENPO
CENPN
CENPU
CENPP
CENPL
CENPH
CENPQ
CENPI
CENPM
CENPR
INCENP
MIS12
DSN1
NSL1
MIS18BP1
PLK1
NDC80
NUF2
CASC5
Centromere and kinetochore proteins
F
Cell Cycle
Chromatin organization
SUMOylation
Cellular response to DNA damage stimulus
Nucleus organization
Regulation of DNA metabolic process
Histone modification
Chromosome maintenance
Regulation of cell cycle process
Regulation of chromosome organization
DNA repair
0
10
20
30
40
50
60
P value (-Log)10
G
WT
CENP-A^AID +IAA
CENP-B-/-
CENP-B-/- CENP-A^AID +IAA
TOP2A
TOP2B
DNA topology and repl. termination
BLM
FANCD2
RIF1
TOPBP1
UFB resolution
SLX4
SLX4IP
Structure-specific endonucleases
ERCC4
ERCC5
ERCC6
UNG
XPC
Nucleotide Excision Repair
MSH3
Mismatch repair
SLF1
SLF2
Post-replication repair
PCNA
POLA1
POLA2
POLD3
RAD18
REV3L
RFC4
POLK
Replisome and Translesion DNA synthesis

Figure 4

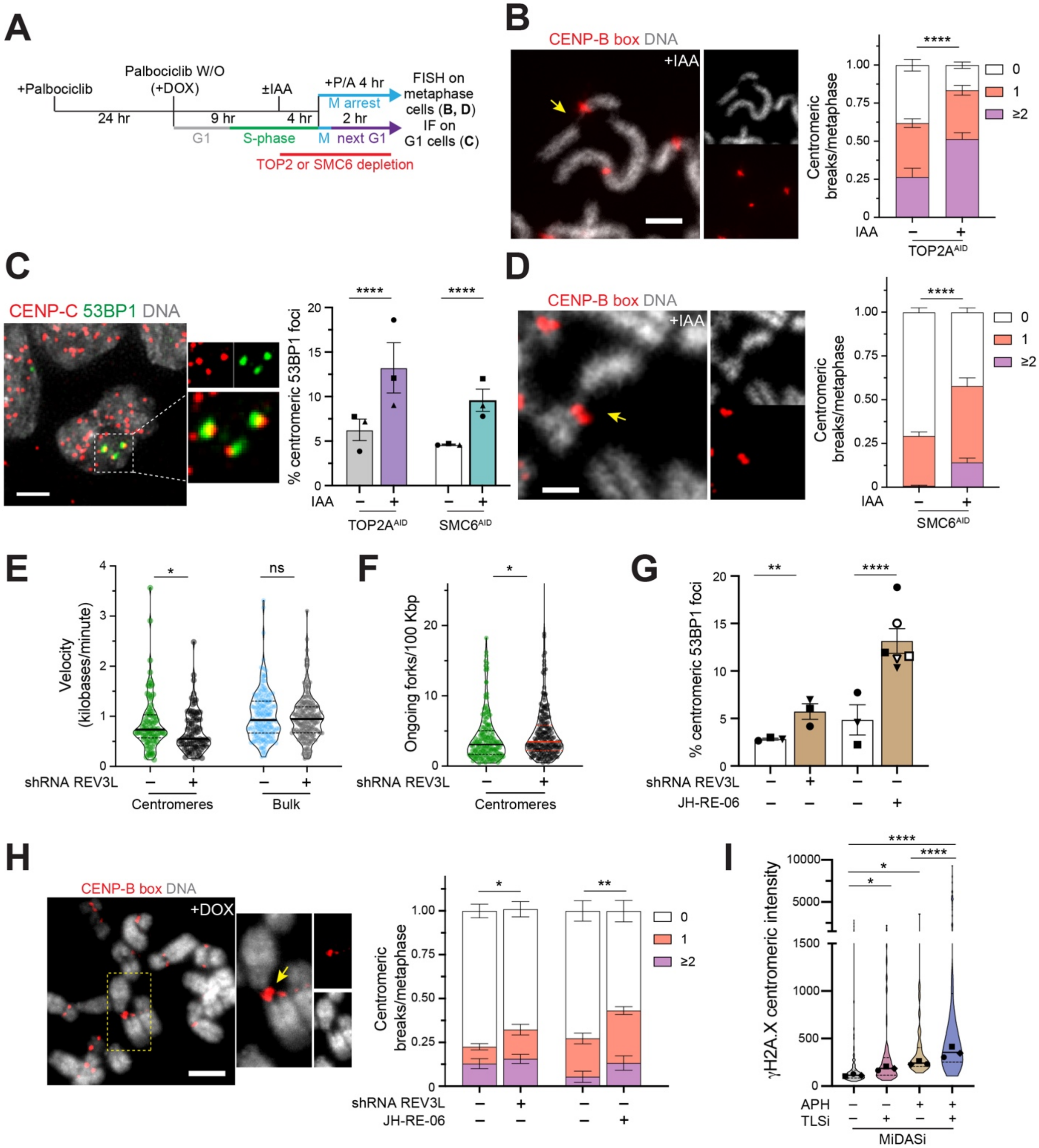
A
+Palbociclib
Palbociclib W/O (+DOX)
±IAA
+P/A 4 hr
M arrest
FISH on metaphase cells (B, D)
IF on G1 cells (C)
24 hr
9 hr
4 hr
2 hr
G1
S-phase
M
next G1
TOP2 or SMC6 depletion
B
CENP-B box DNA
+IAA
Centromeric breaks/metaphase
****
0
1
≥2
IAA
TOP2A^AID
C
CENP-C 53BP1 DNA
% centromeric 53BP1 foci
****
****
IAA
TOP2A^AID
SMC6^AID
D
CENP-B box DNA
+IAA
Centromeric breaks/metaphase
****
0
1
≥2
IAA
SMC6^AID
E
Velocity (kilobases/minute)
*
ns
shRNA REV3L
Centromeres
Bulk
F
Ongoing forks/100 Kbp
*
shRNA REV3L
Centromeres
G
% centromeric 53BP1 foci
**
****
shRNA REV3L
JH-RE-06
H
CENP-B box DNA
+DOX
Centromeric breaks/metaphase
*
**
0
1
≥2
shRNA REV3L
JH-RE-06
I
γH2A.X centromeric intensity
****
****
*
*
APH
TLSi
MiDASi

Figure 5

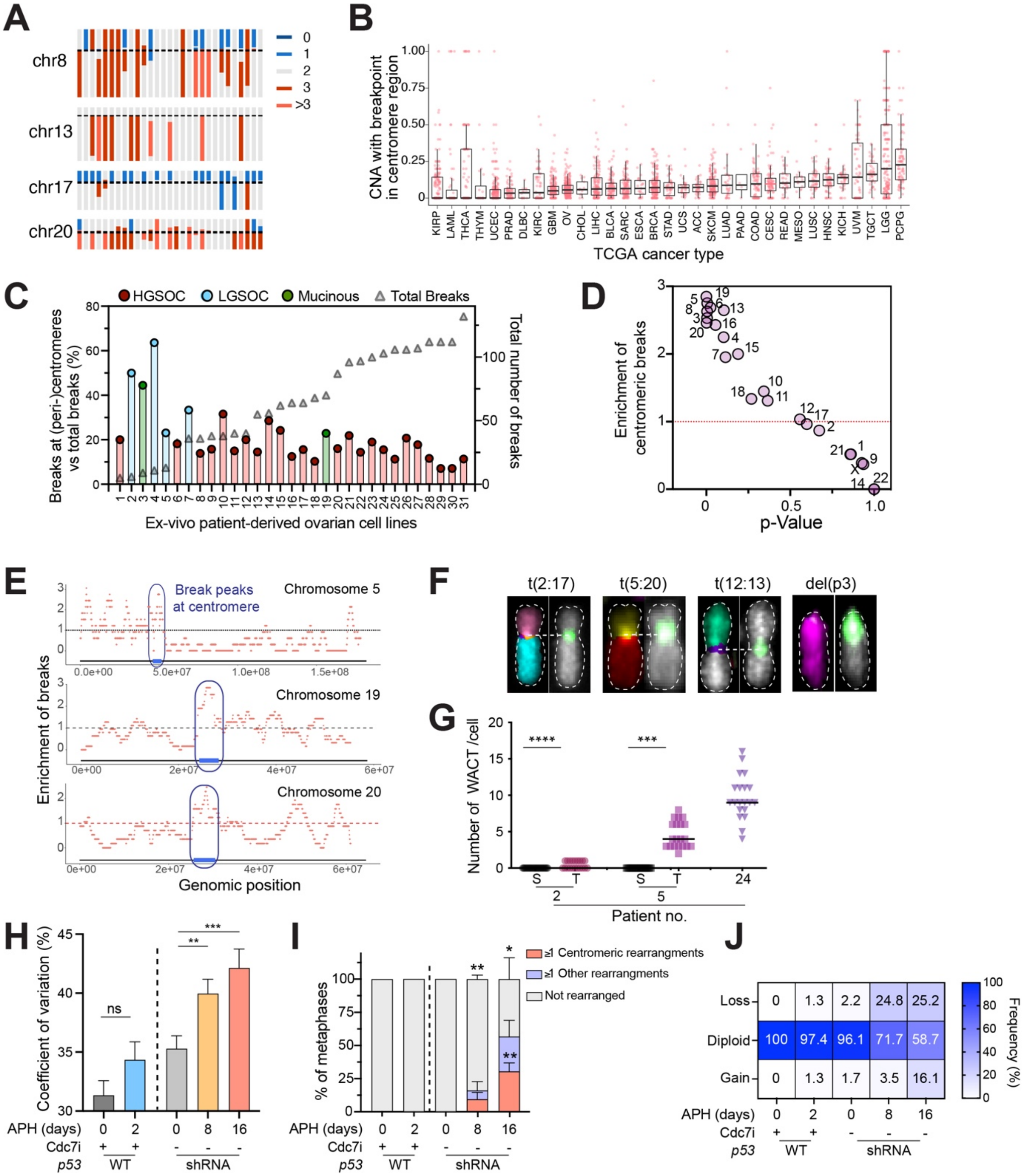
A
chr8
chr13
chr17
chr20
0
1
2
3
>3
B
CNA with breakpoint in centromere region
1.00
0.75
0.50
0.25
0
KIRP LAML THCA THYM UCEC PRAD DLBC KIRC GBM OV CHOL LIHC BLCA SARC ESCA BRCA STAD UCS ACC SKCM LUAD PAAD COAD CESC READ MESO LUSC HNSC KICH UVM TGCT LGG PCPG
TCGA cancer type
C
HGSOC
LGSOC
Mucinous
Total Breaks
Breaks at (peri-)centromeres vs total breaks (%)
Total number of breaks
Ex-vivo patient-derived ovarian cell lines
D
Enrichment of centromeric breaks
p-Value
E
Break peaks at centromere
Chromosome 5
Chromosome 19
Chromosome 20
Enrichment of breaks
Genomic position
F
t(2:17)
t(5:20)
t(12:13)
del(p3)
G
Number of WACT /cell
****
***
S
T
2
5
24
Patient no.
H
Coefficient of variation (%)
ns
**
***
APH (days)
Cdc7i
p53
WT
shRNA
I
% of metaphases
≥1 Centromeric rearrangments
≥1 Other rearrangments
Not rearranged
APH (days)
Cdc7i
p53
WT
shRNA
J
Loss
Diploid
Gain
0 1.3 2.2 24.8 25.2
100 97.4 96.1 71.7 58.7
0 1.3 1.7 3.5 16.1
Frequency (%)
APH (days)
Cdc7i
p53
WT
shRNA

Figure 6

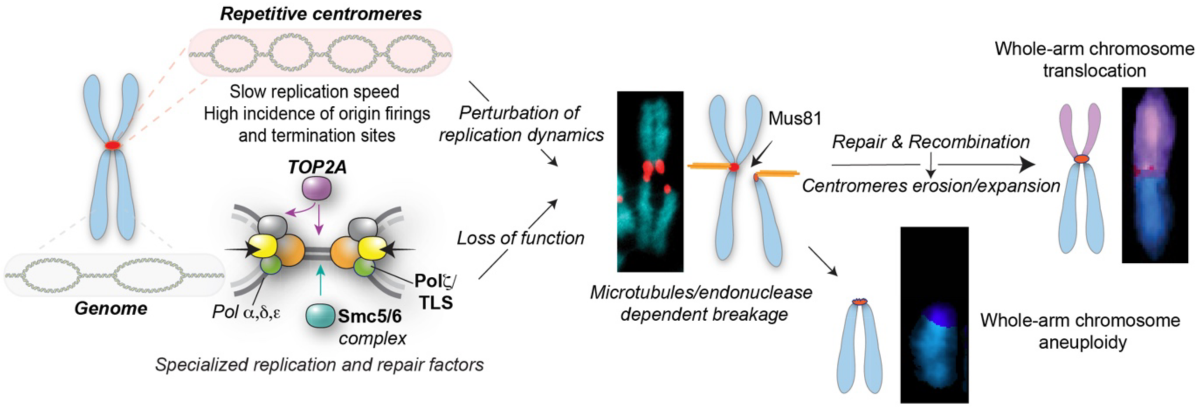
Repetitive centromeres
Slow replication speed
High incidence of origin firings
and termination sites
Perturbation of
replication dynamics
TOP2A
Loss of function
Genome
Pol α,δ,ε
Smc5/6
complex
Polζ/
TLS
Specialized replication and repair factors
Mus81
Microtubules/endonuclease
dependent breakage
Repair & Recombination
Centromeres erosion/expansion
Whole-arm chromosome
translocation
Whole-arm chromosome
aneuploidy

Figure 7

Specialized replication mechanisms maintain genome stability at human centromeres

Andrea Scelfo[1*], Annapaola Angrisani[1*], Marco Grillo[1], Bethany M. Barnes[2], Francesc Muyas[3], Carolin M. Sauer[3], Chin Wei Brian Leung[4], Marie Dumont[1], Marine Grison[1], David Mazaud[5,6], Mickaël Garnier[5,6], Laetitia Guintini[7], Louisa Nelson[2], Fumiko Esashi[4], Isidro Cortés-Ciriano[3], Stephen S. Taylor[2], Jérôme Déjardin[7], Therese Wilhelm[1,#] and Daniele Fachinetti[1,#]

The supplementary data includes:

7 supplementary figures

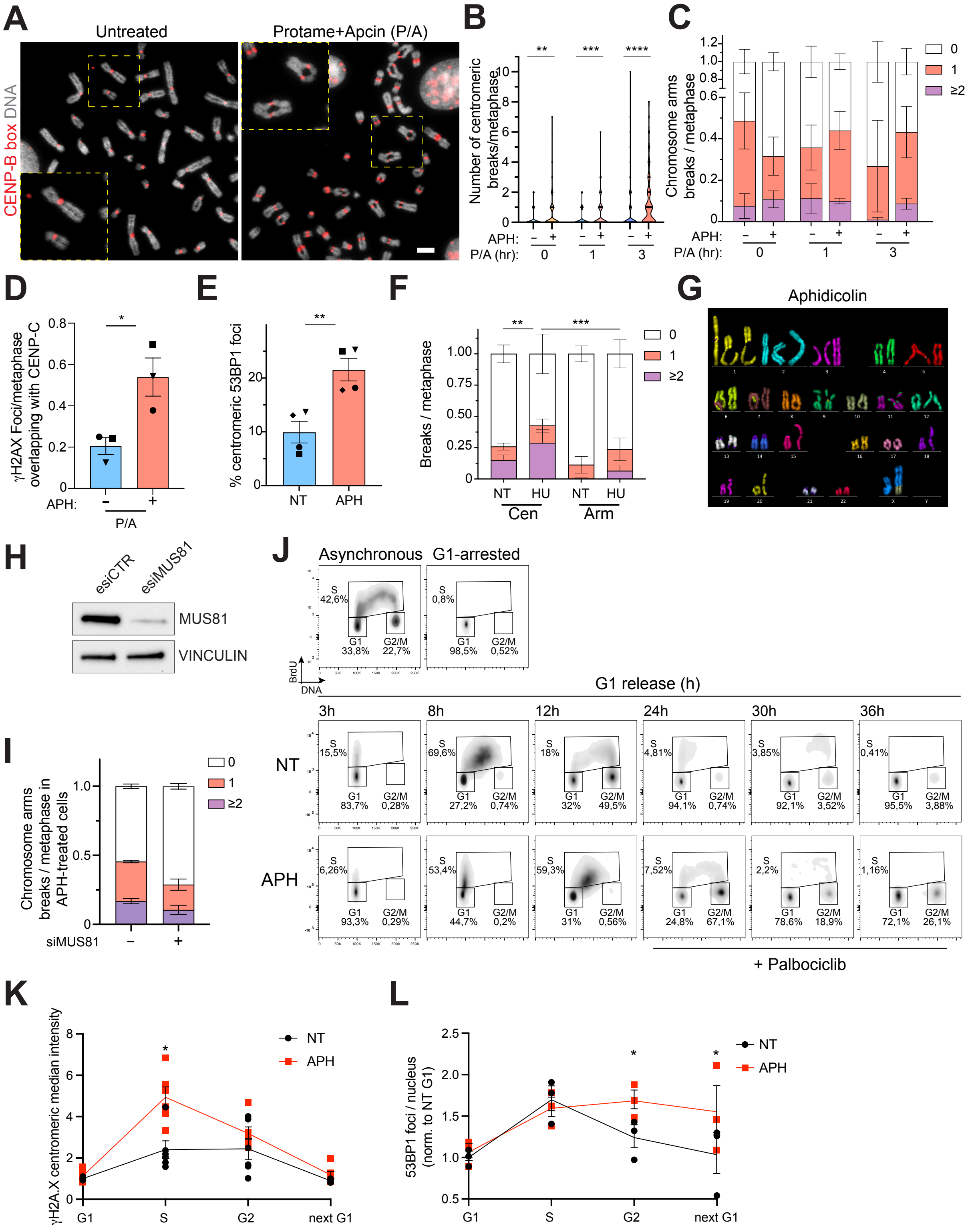

Supplementary Figure 1. Human centromeres break under replication stress. Related to figure 1.

A. Representative images of centromeric FISH (CENP-B box probe) on chromosome spreads from P/A-treated or untreated RPE-1 cells. Scale bar = 10 µm. Yellow squares mark a zoomed region.

B. Quantification of number of breaks/ metaphase at centromeres in the indicated conditions. N = 3, n = 26-92 analyzed metaphases/experiment (see table S3). Unpaired t-test **p = 0.0017, ***p = 0.0010, ****p < 0.0001.

C. Quantification of chromosome arm breaks per observed metaphase in the indicated conditions. The fractions of analyzed metaphases showing 0, 1 and ≥2 centromere breaks are represented. N = 3, n = 26-92 analyzed metaphases/experiment (see table S3). Error bars represent the SEM.

D. Quantification of centromeric γH2A.X foci per nucleus in the indicated conditions. Each dot represents one experiment depicted with a different shape (N = 3, n = 29-45 analyzed metaphases/experiment, see table S3); error bars represent SEM. Unpaired t-test *p = 0.0294.

E. Quantification of centromeric 53BP1 foci (N = 4, n = 52-128 analyzed interphase/experiment, see table S2) in APH-treated cells compared to not treated control (NT). Each dot represents one experiment depicted with a different shape. Unpaired t-test **p = 0.0069.

F. Quantification of breaks per metaphase in not treated control (NT) or HU-treated cells with P/A treatment (3hr), at centromere and chromosome arms. The fractions of analyzed metaphases showing 0, 1 and ≥ 2 centromere breaks are represented. N = 3, n = 49-74 analyzed metaphases/experiment (see table S3). Error bars represent the SEM. χ^2 test (breaks vs non-breaks) **p = 0.0020; ***p = 0.0002.

G. Representative mFISH karyotype of RPE-1 cells treated with APH (200 nM, 24h).

H. Immunoblot with the indicated antibodies of RPE-1 transfected with siRNA (72 h) against a scrambled or MUS81 coding sequence. VINCULIN served as loading control.

I. Quantification of chromosome arms breaks per observed metaphase in MUS81-depleted cells compared to a scrambled control. The fractions of analyzed metaphases showing 0, 1 and ≥ 2 centromere breaks are represented. Cells were treated with 200 nM of APH for 24 h. N = 3, n = 65-71 analyzed metaphases/experiment (see table S3); error bars represent the SEM.

J. Representative cell cycle FACS profiles of synchronized RPE-1 cells according to the schematics shown in Figure 1H.

K. Quantification of centromeric γH2A.X intensity at different cell cycle phases in synchronized RPE-1 cells untreated and APH-treated (200 nM). Cells in the indicated cell cycle phases were obtained fixing cells at different hours from G1 release (Palbociclib washout); to block cells in the next G1, Palbociclib was added during G2. Data are normalized to G1 NT values. Dots represent the mean of >3 experiments and error bars represent the SEM (see table S3). n = an average of 46 cells/experiment was analyzed per condition. Unpaired t-test *p = 0.0308.

L. Quantification of centromeric 53BP1 foci per nucleus at different cell cycle phases in synchronized RPE-1 cells untreated and APH-treated (200 nM). Cells in the indicated cell cycle phases were obtained as in K. Dots represent the mean of 3 experiments and error bars represent the SEM (see table S3). n = an average of 41 cells/experiment was analyzed per condition. Unpaired t-test on total foci *p =0.0269, 0.0208.

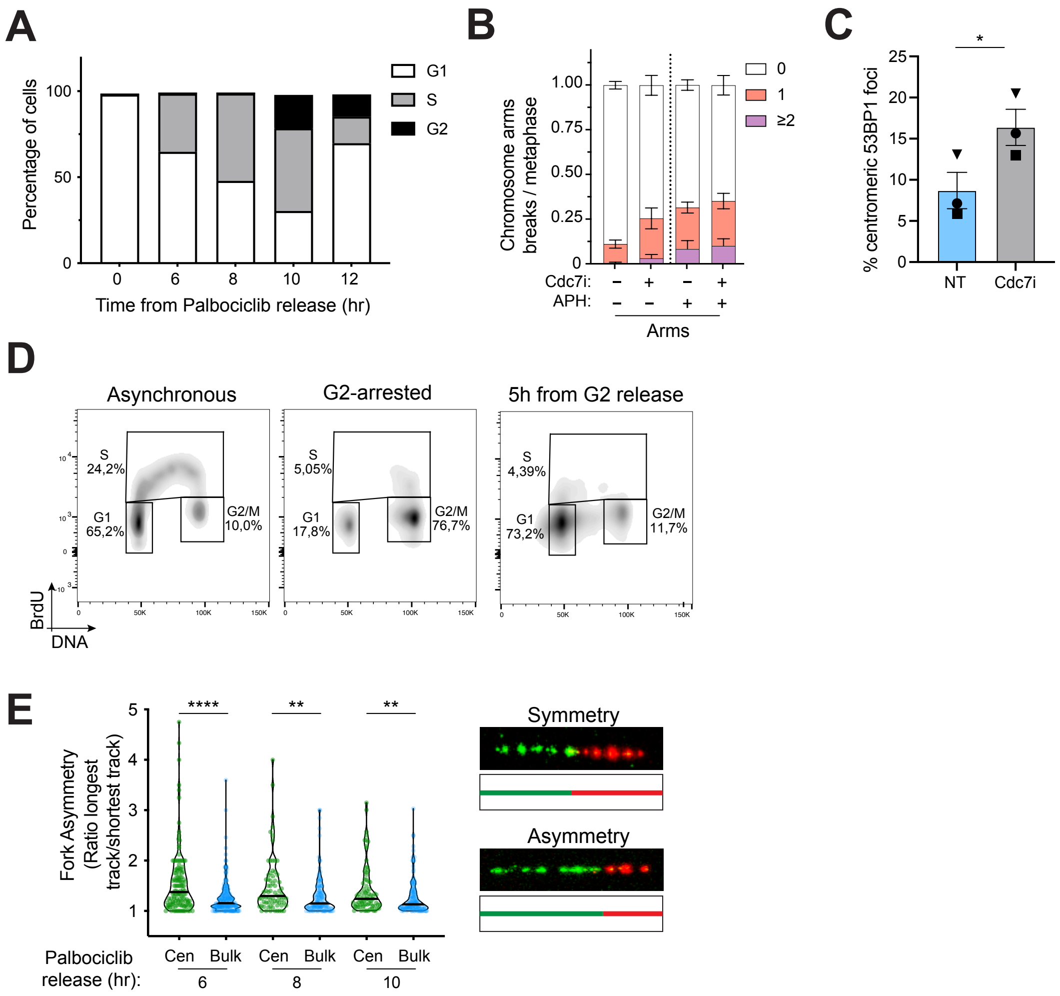

Supplementary Figure 2. Perturbing centromere replication dynamics triggers centromere instability. Related to Figure 2.

A. Cell cycle analysis of RPE-1 cells at indicated times after release from Palbociclib-mediated G1 arrest. S-phase was detected by 30 min BrdU pulse.

B. Quantification of chromosome arms breaks per observed metaphase in the indicated conditions (with P/A treatment). The fractions of analyzed metaphases showing 0, 1 and ≥2 centromere breaks are represented. N = 3 and 4, n = 30-86 analyzed metaphases/experiment (see table S3). Dotted lines separate independent experiments. Error bars represent the SEM.

C. Quantification of centromeric 53BP1 foci (N = 3; n = 57-105 analyzed interphase cell/experiment, see table S3) in Cdc7i-treated cells compared to not treated control (NT). Each dot represents one experiment depicted with a different shape. χ^2 test (breaks vs non-breaks) *p = 0.0157.

D. Representative cell cycle FACS profiles of synchronized RPE-1 cells according to the schematics shown in Figure 2 I.

E. Quantification of fork asymmetry (expressed as the ratio between the longest and the shortest distance covered by replication forks during IdU-CldU pulse-labelling) measured at centromere and bulk DNA at the indicated time after release from G1 arrest by Palbociclib. N = 3, n = 73-218 analyzed DNA fibers per condition (see table S3). The black bars represent the median. Mann–Whitney U test: **p = 0.0014, 0.0035,****p < 0.0001. Right: Representative images of fork symmetry (top) and asymmetry (bottom).

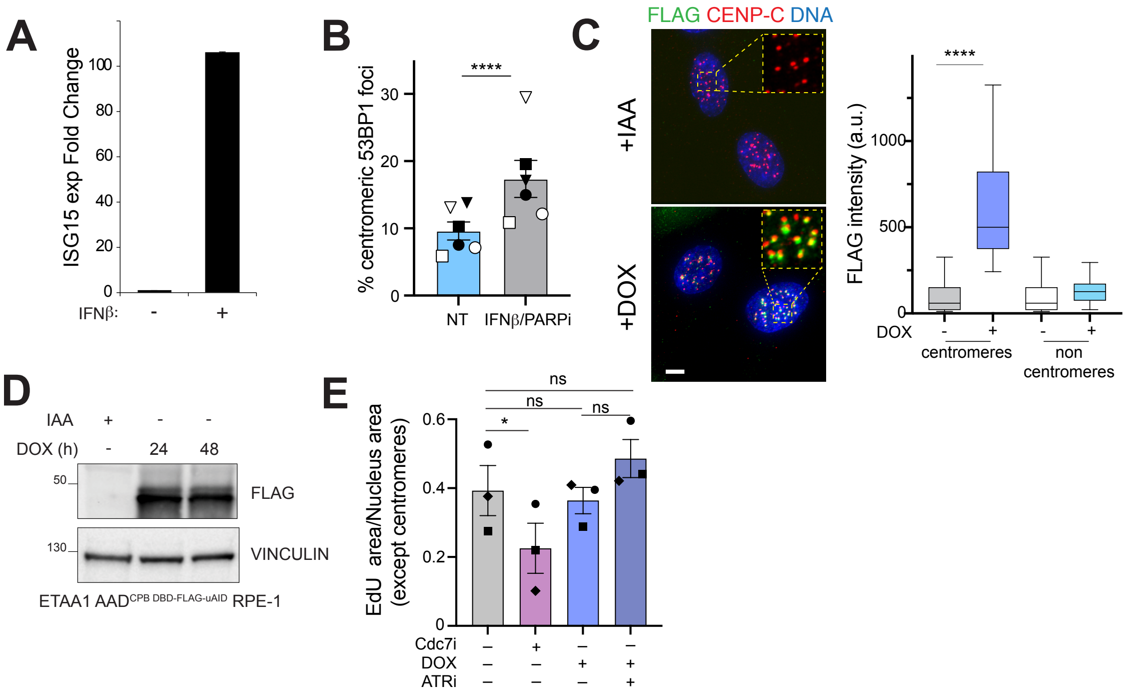

Supplementary Figure 3. Perturbing centromeric replication leads to centromeric damage. Related to Figure 3.

A. mRNA expression level of ISG15 measured by RT-qPCR in RPE-1 treated with 30U/mL IFNβ for 2 hr and released for 48 hr, normalized to GAPDH and to untreated control (ΔΔCt). Error bars represent the SEM.

B. Quantification of centromeric 53BP1 foci (N = 3, n = 57-114 analyzed interphase cell/experiment, see table S2) in either IFNβ- or PARPi-treated cells compared to not treated control (NT). Each dot represents one experiment depicted with a different shape (INFβ: solid symbols; PARPi: open symbols). χ^2 test (breaks vs non-breaks) ****p < 0.0001.

C. Representative images of Flag-tagged ETAA1$^{\text{CB-DBD}}$ protein (dox 48 h, 100 ng/mL) (left) and relative quantification (right) at centromere compared to random regions. n >23 analyzed cells. Scale bar = 10 µm. Unpaired t-test ****p < 0.0001.

D. Immunoblot analyses showing Flag-tagged ETAA1$^{CB\text{-}DBD}$ protein expression at the indicated times from induction with doxycycline treatment. VINCULIN served as loading control.

E. Quantification of nuclear, non-centromeric EdU area in RPE-1 ETAA1$^{CB\text{-}DBD}$ cells treated as indicated for 24 h (Dox: 100 ng/mL, Cdc7i, ATRi: 10 μM). Dots depicted with different shape represent the mean value of one experiment. N = 3, n = > 5 analyzed cells; error bars represent the error to the mean for one condition (see Methods). Holm post hoc test: * = 0.050.

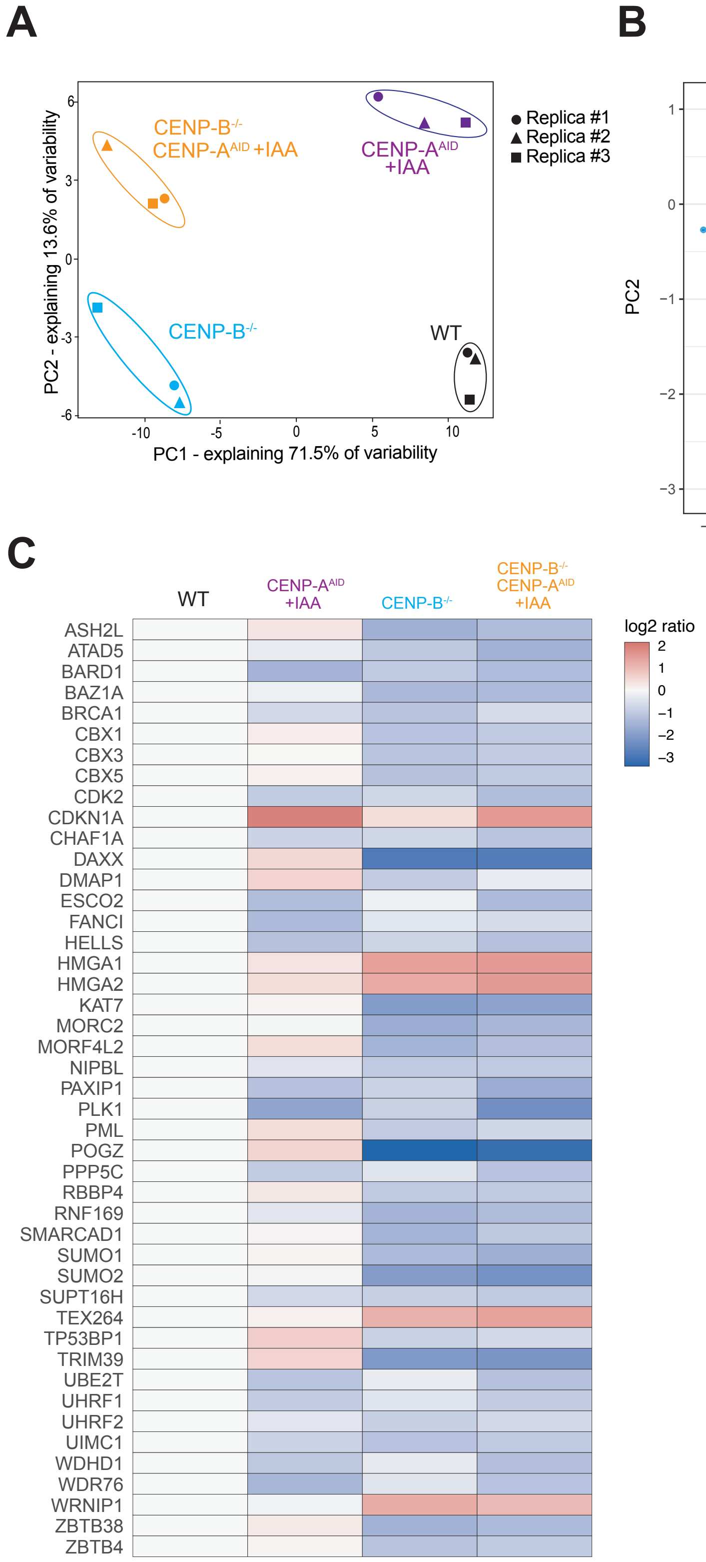

Supplementary Figure 4. Quantitative proteomics of human centromere reveals the presence

of DNA damage and repair factors. Related to figure 4.

A. Principal Component Analysis (PCA) of the proteomics values from TMT-PICh performed in the indicated cell lines to visualise the relationship among the samples. Dashed circles enclose experimental replicates.

B. PCA Cluster analysis (hierarchical clustering) of hits and candidates proteins showing ten distinct clusters. Centromere and kinetochore proteins form a discrete cluster highlighted by dashed circle.

C. Heat map showing selected centromeric proteins regulated among the indicated conditions identified by the PICh involved in DNA damage, DNA repair and replication.

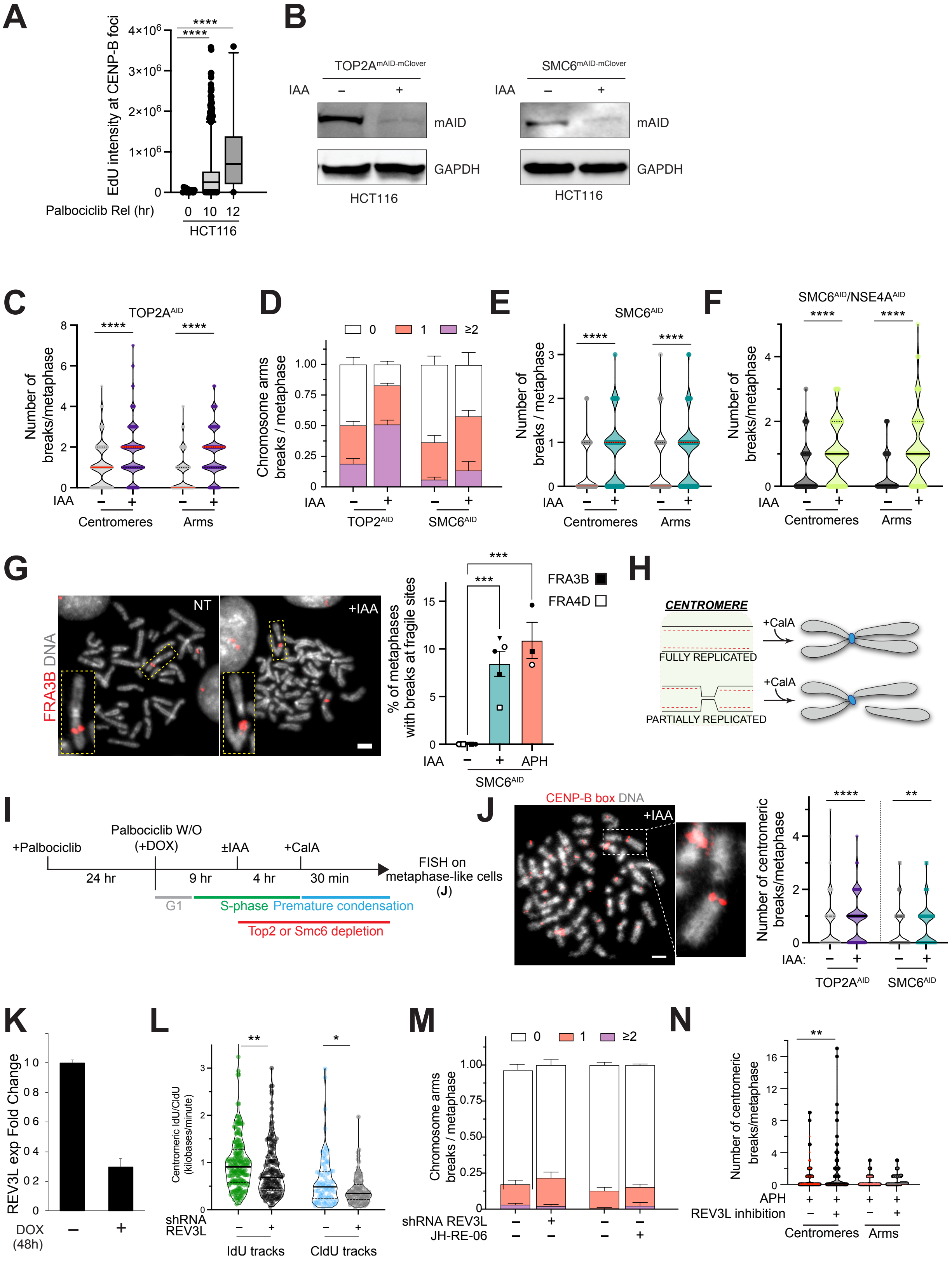
A
EdU intensity at CENP-B foci
4×10^6
3×10^6
2×10^6
1×10^6
0
****
****
Palbociclib Rel (hr)
0
10
12
HCT116
B
TOP2A mAID-mClover
SMC6 mAID-mClover
IAA
–
+
mAID
GAPDH
HCT116
C
TOP2A AID
Number of breaks/metaphase
****
****
IAA
Centromeres
Arms
D
0
1
≥2
Chromosome arms breaks / metaphase
1.00
0.75
0.50
0.25
0
TOP2 AID
SMC6 AID
E
SMC6 AID
Number of breaks / metaphase
Centromeres
Arms
F
SMC6 AID/NSE4A AID
Number of breaks/metaphase
Centromeres
Arms
G
FRA3B DNA
NT
+IAA
% of metaphases with breaks at fragile sites
***
***
FRA3B
FRA4D
APH
SMC6 AID
H
CENTROMERE
+CalA
FULLY REPLICATED
PARTIALLY REPLICATED
I
+Palbociclib
Palbociclib W/O (+DOX)
±IAA
+CalA
24 hr
9 hr
4 hr
30 min
FISH on metaphase-like cells (J)
G1
S-phase
Premature condensation
Top2 or Smc6 depletion
J
CENP-B box DNA
+IAA
Number of centromeric breaks/metaphase
****
**
IAA:
TOP2A AID
SMC6 AID
K
REV3L exp Fold Change
1.0
0.8
0.6
0.4
0.2
0
DOX (48h)
L
Centromeric IdU/CldU (kilobases/minute)
**
*
shRNA REV3L
IdU tracks
CldU tracks
M
0
1
≥2
Chromosome arms breaks / metaphase
shRNA REV3L
JH-RE-06
N
Number of centromeric breaks/metaphase
**
16
12
8
4
0
APH
REV3L inhibition
Centromeres
Arms

Supplementary Figure 5. TOP2A, SMC5/6 and Translesion Synthesis Polymerases maintain centromere stability. Related to Figure 5.

A. Intensity of EdU signal (A.U.) measured at CENP-B foci after release (hr) from Palbociclib-mediated G1 arrest. Error bars represent the standard error of the mean. Unpaired t test: ****p < 0.0001.

B. Immunoblot analyses with the indicated antibodies showing TOP2A and SMC6 IAA-induced depletion (8h) compared to untreated control, treated according to the schematics of Figure 4A. GAPDH served as loading control.

C. Violin plot showing quantification of breaks at centromeres and chromosome arms per metaphase in untreated or IAA treated cells. N = 7, n = 28-63 analyzed metaphases/experiment (see table S3). Unpaired t-test ****p < 0.0001.

D. Quantification of chromosome arms breaks per observed metaphase in the indicated conditions. The fractions of analyzed metaphases showing 0, 1 and ≥2 centromere breaks are represented. N = 7 or 4, n = 28-70 analyzed metaphases/experiment (see table S3). Error bars represent the standard error of the mean (SEM).

E, F. Violin plots showing quantification of breaks at centromeres and chromosome arms per metaphase in untreated or IAA treated cells in (E) SMC6^{AID} cells and (F) SMC6^{AID}; NSE4A^{AID} cells. N = 4 and 2, n = 28-63 and 54-65 analyzed metaphases/experiment, respectively (see table S3). Unpaired t-test ****p < 0.0001.

G. (Left) Representative image of FISH against FRA3B fragile sites and relative quantification (right) in NT, SMC6-depleted and APH-treated cells. Each dot represents one experiment depicted with a different shape (n = 20 analyzed cells/experiment, see table S3). Unpaired t-test ***p = 0.0002. Scale bar = 10 μm

H, I. (H) Schematic of the scope of the experiment with (I) relative experimental plan. W/O: washout; IAA: Auxin; CalA: Calyculin A.

J. (Left) Representative image of FISH against CENP-B box and relative violin plots (right) showing quantification of breaks at centromeres per metaphase in untreated or IAA-treated cells, in presence of CalA treatment (50 ng/mL) in the indicated cell lines. N = 4 or 5, n = 30-72 analyzed metaphases/experiment (see table S3). Unpaired t-test $^{**}p = 0.0032$, $^{****}p < 0.0001$.

K. mRNA expression level of REV3L measured by RT-qPCR in RPE-1 treated with DOX (48 hr) normalized to GAPDH and to untreated control ($\Delta\Delta$Ct). Error bars represent the SEM.

L. Quantification of the replication fork velocity measured at centromeric DNA in untreated and doxycycline-induced REV3L depleted RPE-1 after release (10 h) from G1 arrest by Palbociclib. n=80-184 analyzed DNA fibers per condition (see table S3). Dark bars indicate the median, dashed lines the interquartiles. Mann–Whitney U test: $^{*}p = 0.0117$, $^{**}p = 0.0010$.

M. Quantification of chromosome arms breaks per observed metaphase in the indicated conditions. The fractions of analyzed metaphases showing 0, 1 and ≥ 2 centromere breaks are represented. N = 3, n = 31-84 analyzed metaphases/experiment (see table S3). Error bars represent the standard error of the mean (SEM).

N. Violin plots showing quantification of breaks at centromeres and chromosome arms per metaphase after REV3L doxycycline-induced depletion or JH-RE-06-mediated inhibition in combination with 100 nM APH treatment N = 5, n = 51-88 analyzed metaphases/experiment (see table S3). Unpaired t-test $^{**}p = 0.0067$.

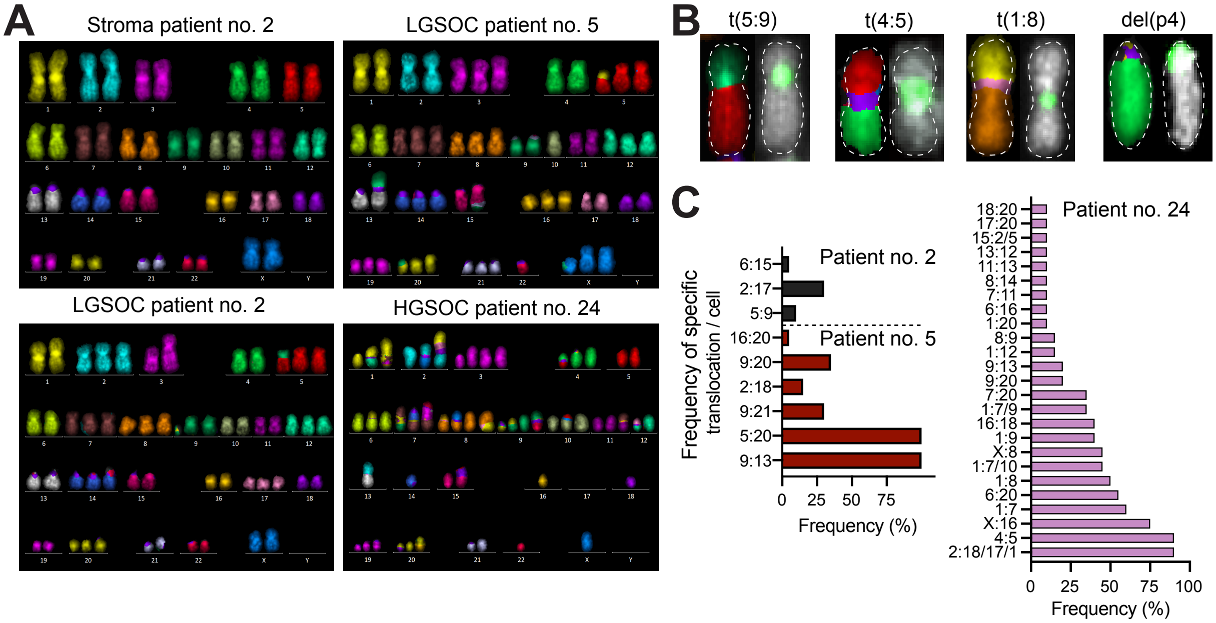

Supplementary Figure 6. Chromosomal alterations involving centromeres in ex-vivo tumor-derived cells. Related to Figure 6.

A. Representative mFISH karyotypes of patient-derived LGSOC tumor and stromal cells and HGSOC tumour cells.

B. Representative images of whole-arm chromosome translocation in OCMs from patients #2, #5 and 24 visualized by mFISH followed by a centromeric FISH (CENP-B box probe in green).

C. Column bar graphs show the frequency of the observed WACT in the indicated tumour samples. n = 20 analyzed metaphases/experiment.

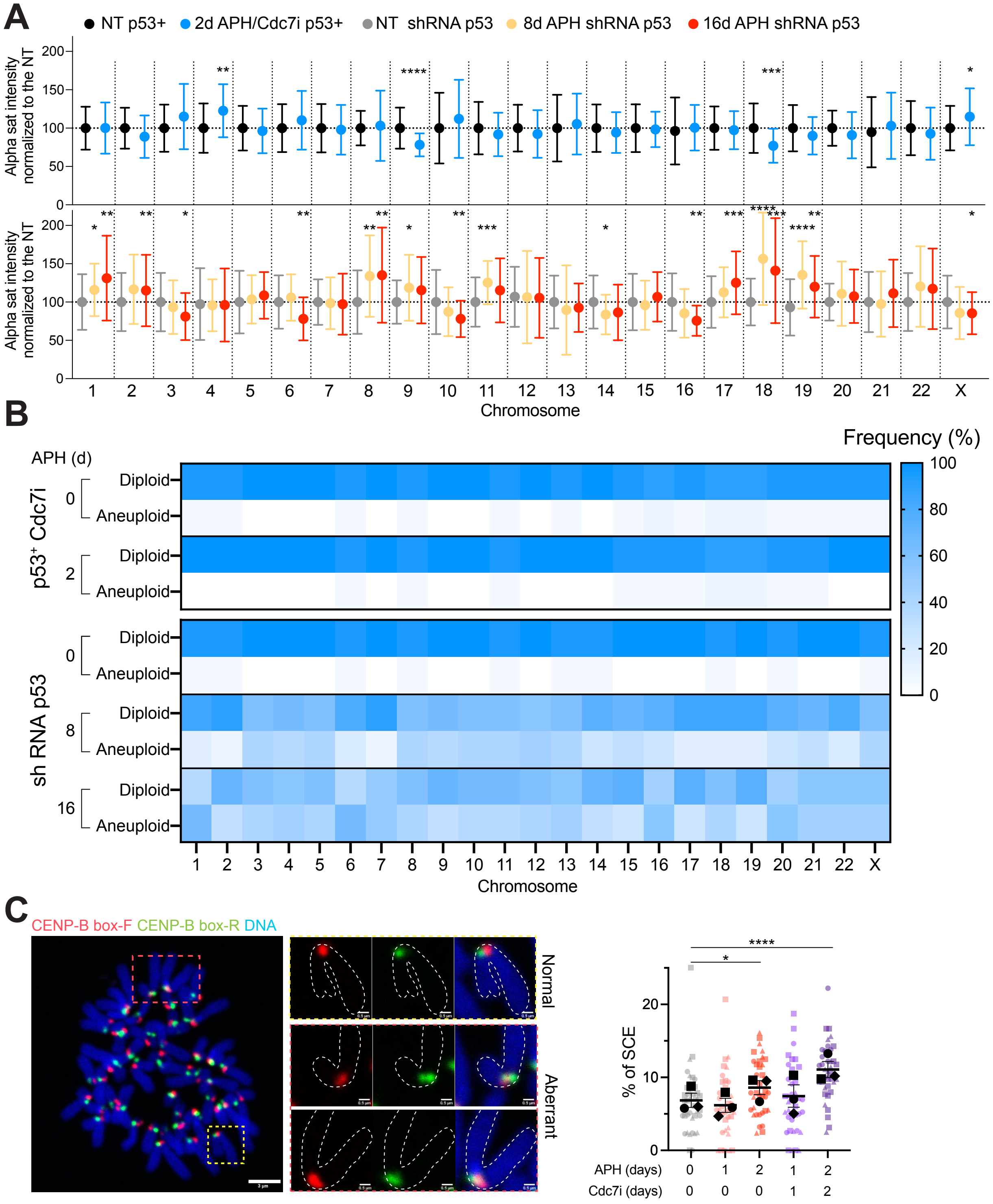

Supplementary Figure 7. Prolonged replication stress induces centromeric alterations and aneuploidy. Related to Figure 6 and 7.

A. Measurements of alpha-satellite intensity measured at individual chromosomes of WT and p53 shRNA RPE-1 cells treated as indicated (APH 2 days: 200 nM; 8 and 16 days: 100 nM. Cdc7i: 10µM). Values are normalized to non-treated condition. Error bars represent the SEM. N = 22, n = 20 analyzed cells**.** Unpaired t-test ns *0.05 < p < 0.01, **: 0.001 < p < 0.01, ***: 0.0001 < p < 0.001, ****: p < 0.0001.

B. Frequency of specific chromosome aneuploidy measured at individual chromosomes of WT and p53 shRNA RPE-1 cells treated as indicated (APH 2 days: 200 nM; 8 and 16 days: 100 nM. Cdc7i: 10µM). N = 2, n = 20 analyzed cells**.**

C. Representative images of cen-co-FISH analysis (left) and percentage of sister chromatid exchange (SCE) (right) measured in RPE-1 cells treated as indicated (APH 200 nM; Cdc7i: 10µM). Dots depicted with different shape represent the mean value of one experiment. N = 3, n =12 analyzed metaphases/experiment (see table S3); error bars represent the SEM. Unpaired t-test *p = 0.0398; ****p < 0.0001.